NAVAL POSTGRADUATE SCHOOL
MONTEREY, CALIFORNIA

THESIS

INVESTIGATION OF A CONSTRICTED ANNULAR ACOUSTIC RESONATOR

by

Choe, Seok Yun

June, 1997

Thesis Advisor: Anthony A. Atchley
Co-Advisor : Ralph T. Muehleisen

Approved for public release; distribution is unlimited.

REPORT DOCUMENTATION PAGE

Form Approved OMB No. 0704-0188

1. AGENCY USE ONLY *(Leave blank)*	2. REPORT DATE June 1997	3. REPORT TYPE AND DATES COVERED Master's Thesis

4. TITLE AND SUBTITLE
INVESTIGATION OF A CONSTRICTED ANNULAR ACOUSTIC RESONATOR

5. FUNDING NUMBERS

6. AUTHOR(S)
Choe, Seok Yun

7. PERFORMING ORGANIZATION NAME(S) AND ADDRESS(ES)
Naval Postgraduate School
Monterey CA 93943-5000

8. PERFORMING ORGANIZATION REPORT NUMBER

9. SPONSORING/MONITORING AGENCY NAME(S) AND ADDRESS(ES)

10. SPONSORING/MONITORING AGENCY REPORT NUMBER

11. SUPPLEMENTARY NOTES The views expressed in this thesis are those of the author and do not reflect the official policy or position of the Department of Defense or the U.S. Government.

12a. DISTRIBUTION/AVAILABILITY STATEMENT
Approved for public release; distribution is unlimited.

12b. DISTRIBUTION CODE

13. ABSTRACT *(maximum 200 words)*

One topic of current interest in thermoacoustic research is an annular prime mover [Lin et al., J. Acoust. Soc. Am, 100, 2846 (1996)]. The starting point for this research is an investigation of a constricted annular resonator. A literature search of the field resulted in surprisingly few references. The results of analytic, numerical, and experimental investigations are presented. Introducing a constriction into an annular resonator splits each longitudinal duct mode into two modes, one of a higher frequency with a pressure antinode at the constriction and one at a lower frequency with a velocity antinode near the constriction. The lower mode is more sensitive to changes in the length and porosity of the constriction than the higher mode. Overall agreement between measured and predicted mode shapes and resonance frequencies is very good. It was found that it is necessary to include end corrections at the constriction to get accurate agreement between measured and predicted results.

14. SUBJECT TERMS
acoustics: annular resonator, end corrections, mode splitting

15. NUMBER OF PAGES 88

16. PRICE CODE

17. SECURITY CLASSIFICATION OF REPORT	18. SECURITY CLASSIFICATION OF THIS PAGE	19. SECURITY CLASSIFICATION OF ABSTRACT	20. LIMITATION OF ABSTRACT
Unclassified	Unclassified	Unclassified	UL

NSN 7540-01-280-5500

Standard Form 298 (Rev. 2-89)
Prescribed by ANSI Std. 239-18 298-102

Approved for public release; distribution is unlimited.

INVESTIGATION OF A CONSTRICTED ANNULAR ACOUSTIC RESONATOR

Choe, Seok Yun
Lieutenant Commander, Korean Navy
B.S., Korean Naval Academy, 1987

Submitted in partial fulfillment
of the requirements for the degrees of

MASTER OF SCIENCE IN ENGINEERING ACOUSTICS

from the

NAVAL POSTGRADUATE SCHOOL
June 1997

Author: _____
Choe, Seok Yun

Approved by: _____
Anthony A. Atchley, Thesis Advisor

_____
Ralph T. Muehleisen, Co-Advisor

_____
Robert Keolian, Chairman
Engineering Acoustics Academic Committee

ABSTRACT

One topic of current interest in thermoacoustic research is an annular prime mover [Lin et al., J. Acoust. Soc. Am, 100, 2846 (1996)]. The starting point for this research is an investigation of a constricted annular resonator. A literature search of the field resulted in surprisingly few references. The results of analytic, numerical, and experimental investigations are presented. Introducing a constriction into an annular resonator splits each longitudinal duct mode into two modes, one of a higher frequency with a pressure antinode at the constriction and one at a lower frequency with a velocity antinode near the constriction. The lower mode is more sensitive to changes in the length and porosity of the constriction than the higher mode. Overall agreement between measured and predicted mode shapes and resonance frequencies is very good. It was found that it is necessary to include end corrections at the constriction to get accurate agreement between measured and predicted results.

TABLE OF CONTENTS

I. INTRODUCTION

The purpose of this thesis is to investigate acoustic resonances in a constricted, annular resonator. The motivation for this project is based on a related problem in the area of thermoacoustis - the annular prime mover. The intent is that the measurements reported in this thesis will serve as preliminary validation of models being developed for the prime mover project.

The azimuthal modes of a uniform cross section annulus are degenerate. The introduction of a constriction splits the degeneracy resulting in two modes having different resonance frequencies and distributions of acoustic pressure (mode shape). The goal of this thesis is to both measure and predict the frequency splitting and mode shapes.

A theoretical discussion will be covered in the Chapter II. Chapter III is a description of the experimental apparatus including the annular acoustic resonator and peripheral equipment. In addition, a detailed discussion of the data collection procedure will be covered. Chapter IV is an analysis of the data obtained and comparison with predictions. The thesis is summarized and important conclusions are addressed in Chapter V.

II. THEORY

A. INTRODUCTION

The purpose of this chapter is to outline the theoretical analysis of a driven, constricted annular resonator. The discussion begins with the solution of the wave equation in and the effective radius of a uniform cross section annular resonator. This solution is developed in cylindrical coordinates. However, because the purpose of this thesis is to investigate frequencies below those required to excite cross modes, we adopt a simplified plane model for the majority of analysis.

The next step is to introduce a constriction. It is shown that the constriction results in frequency splitting of what were degenerated, orthogonal modes in the uniform cross section resonator. It is also shown that the degree to which a particular mode is excited depends upon the location of the driver relative to the constriction. Because of dissipation, the modes overlap in frequency space and, in general, two modes are simultaneously excited. When this situation occurs the resonance frequencies of the individual modes cannot be determined from peaks in the frequency response. However, pole-zeros analysis of the frequency response can yield accurate values for the resonance frequencies. The chapter concludes with a discussion of pole-zero analysis of two coupled modes.

B. SOLUTION FOR A UNIFORM ANNULAR RESONATOR

The analysis begins with the general solution of the acoustic wave equation in cylindrical coordinates

$$\nabla^2 p = \frac{1}{c^2}\frac{\partial^2 p}{\partial t}, \tag{2.1}$$

where

$$\nabla^2 = \frac{1}{r}\frac{\partial}{\partial r}\left(r\frac{\partial}{\partial r}\right) + \frac{1}{r^2}\frac{\partial^2}{\partial \theta} + \frac{\partial^2}{\partial z^2}. \tag{2.2}$$

Assuming harmonic time dependence, the wave equation becomes the Helmholtz equation

$$\nabla^2 \mathrm{P} = -k^2 \mathrm{P} \qquad \text{where} \quad k^2 = \left(\frac{\omega}{c}\right)^2 . \tag{2.3}$$

The general solution of Eq. (2.3) is assumed to be expressed as the product of three terms, each a function of only one variable.

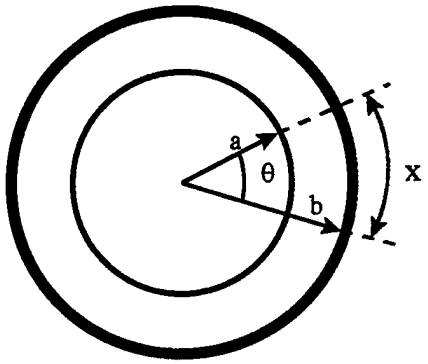

Figure 2-1. Geometry for the annular resonator.

$$\mathrm{P}(r,\theta,z) = R(r)\Theta(\theta)\mathrm{Z}(z) \tag{2.4}$$

Substituting Eq. (2.4) into (2.3) and dividing by $R\Theta\mathrm{Z}$, gives

$$\frac{1}{R}\frac{1}{r}\frac{\partial}{\partial r}\left(r\frac{\partial R}{\partial r}\right) + \frac{1}{r^2}\frac{1}{\Theta}\frac{\partial^2\Theta}{\partial\theta^2} + \frac{1}{\mathrm{Z}}\frac{\partial^2\mathrm{Z}}{\partial z^2} = -k^2 . \tag{2.5}$$

Rearranging to isolate the z-dependent terms gives

$$\frac{1}{R}\frac{1}{r}\frac{\partial}{\partial r}\left(r\frac{\partial R}{\partial r}\right) + \frac{1}{r^2}\frac{1}{\Theta}\frac{\partial^2\Theta}{\partial\theta^2} + k^2 = -\frac{1}{\mathrm{Z}}\frac{\partial^2\mathrm{Z}}{\partial z^2} . \tag{2.6}$$

Following the standard separation of variables solution technique,

let $$\frac{1}{\mathrm{Z}}\frac{\partial^2\mathrm{Z}}{\partial z^2} = -k_z^2 . \tag{2.7}$$

The general solution to this equation is

$$\mathrm{Z} = \mathrm{A}_z \cos(k_z z) + \mathrm{B}_z \sin(k_z z) \tag{2.8}$$

Equation (2.6) now becomes after multiplying through by r^2 and rearranging

$$\frac{r}{R}\frac{\partial}{\partial r}\left(r\frac{\partial R}{\partial r}\right)+\left(k^2-k_z^2\right)r^2=-\frac{1}{\Theta}\frac{\partial^2\Theta}{\partial\theta^2}. \tag{2.9}$$

Let
$$\frac{1}{\Theta}\frac{\partial^2\Theta}{\partial\theta^2}=-m^2. \tag{2.10}$$

The general solution to this equation is conveniently expressed in the form

$$\Theta(\theta)=\cos(m\theta+\phi) \tag{2.11}$$

Equation (2.9) is now reduced to

$$\frac{r}{R}\frac{\partial}{\partial r}\left(r\frac{\partial R}{\partial r}\right)+(k_r^2r^2-m^2)=0, \tag{2.12}$$

where
$$k_r^2=k^2-k_z^2. \tag{2.13}$$

The general solution to this equation is

$$R(r)=A_mJ_m(k_rr)+B_mY_m(k_rr), \tag{2.14}$$

where $J_m(k_rr)$ and $Y_m(k_rr)$ are the cylindrical Bessel and Neumann functions. The Neumann function must be retained because the origin is excluded in our annular resonator.

All boundaries are assumed to be rigid, so the normal component of acoustic velocity must be zero at the boundaries. Applying rigid boundary conditions at $z=0$ and $z=L_z$ implies that $B_z=0$ and

$$k_z=\frac{l\pi}{L_z},\quad l=0,1,2\ldots \tag{2.15}$$

The function $\Theta(\theta)$ must be periodical, in other words, $\Theta(\theta)=\Theta(\theta+2\pi)$. This condition is satisfied if m is an integer, $m=0,1,2\cdots$.

Application of rigid boundary condition at $r=a$ and $r=b$ implies that

$$A_mJ'_m(k_ra)+B_mY'_m(k_ra)=0$$
$$A_mJ'_m(k_rb)+B_mY'_m(k_rb)=0. \tag{2.16}$$

Expressed in matrix form these equations become

$$\begin{pmatrix} J_m'(k_r a) & Y_m'(k_r a) \\ J_m'(k_r b) & Y_m'(k_r b) \end{pmatrix} \begin{pmatrix} A_m \\ B_m \end{pmatrix} = \begin{pmatrix} 0 \\ 0 \end{pmatrix}. \tag{2.17}$$

The values of $k_r a$ that satisfy this equation are those for which the determinant of the first matrix is zero , i.e.

$$J'_m(k_r a)Y'_m(k_r b) - J'_m(k_r b)Y'_m(k_r a) = 0. \tag{2.18}$$

Let the values of $k_r a$ that satisfy Eq. (2.18) be called α_{mn}. With this definition, the first of Eqs. (2.16) becomes

$$B_m = -A_m \frac{J_m'(\alpha_{mn})}{Y_m'(\alpha_{mn})}, \tag{2.19}$$

and Eq. (2.14) becomes

$$R(r) = A_m[J_m(k_r r) - \frac{J_m'(\alpha_{mn})}{Y_m'(\alpha_{mn})} Y_m(k_r r)]. \tag{2.20}$$

For the purposes of this thesis, we are interested in frequencies low compared to those required to excite cross modes. To eliminate pressure variations in the z direction, we require that $l = 0$ in Eq. (2.15). In this case $Z(z) = 1$, and $k_r^2 = k^2$. We are also interested in modes for which the circumference of the resonator is approximately one wavelength long, i.e. m = 1 in Eq. (2.11). Under these conditions, the solution to the Helmholtz equation is

$$P(r,\theta) = A\ [J_1(k_r r) - \frac{J_1'(\alpha_{1n})}{Y_1'(\alpha_{1n})} Y_1(k_r r)]\cos(\theta + \phi). \tag{2.21}$$

The dimensions for our particular resonator are a = 10.00 cm and b = 15.30 cm. The lowest value of α_{mn} is then $\alpha_{10} = 0.796$. Recall that for $l = 0$, $k_r^2 = k^2 = (\frac{2\pi}{\lambda})^2$. Also, $k_r = \frac{\alpha_{10}}{a}$. Combining these expressions for k_r implies that

$$\frac{2\pi}{\lambda} = \frac{\alpha_{10}}{a} \tag{2.22}$$

Let us define the effective circumference of the resonator $L_{eff} = m\lambda$, or for m = 1 $L_{eff} = \lambda$. Combining this definition with the Eq. (2.22) and rearranging yields

$$L_{eff} = \frac{2\pi a}{\alpha_{10}} \tag{2.23}$$

Alternatively, we can define an effective radius $R_{eff} = \frac{L_{eff}}{2\pi}$. Using Eq. (2.23), we have $R_{eff} = \frac{a}{\alpha_{10}}$. For $\alpha_{10} = 0.796$, $R_{eff} = 12.56$ cm.

C. PLANE WAVE THEORY

The parameter R_{eff} is defined in such a way that

$$R_{eff} = \frac{L_{eff}}{2\pi} = \frac{\lambda}{2\pi} = \frac{1}{k}. \tag{2.24}$$

The angular coordinate θ can be related to the arc length x measured at R_{eff} through

$$\theta = \frac{x}{R_{eff}} = kx \ . \tag{2.25}$$

With this definition, the θ - dependence of the acoustic pressure becomes

$$\cos(kx + \phi). \tag{2.26}$$

This function can be expressed in terms of complex exponentials as

$$\cos(kx + \phi) = 2[e^{j(kx+\phi)} + e^{-j(kx+\phi)}], \tag{2.27}$$

Substituting this result into Eq. (2.21) gives

$$P(r,\theta,t) = R(r)[e^{j(\omega t - kx - \phi)} + e^{j(\omega t + kx + \phi)}]. \tag{2.28}$$

The interpretation of Eq. (2.28) is that the pressure is represented by two counter propagating waves that behave essentially like plane waves. This analogy will be used to analyze the nature of the sound field in the annular resonator.

The plane-wave-like solution will be valid for frequencies below those required to excite the first cross mode. The frequencies corresponding to normal modes in the r - z plane are given by

$$f_c = \frac{c}{2\pi}\sqrt{k_r^2 + k_z^2} = \frac{c}{2\pi}\sqrt{(\frac{\alpha_{mn}}{a})^2 + (\frac{l\pi}{L_z})^2}\ . \qquad (2.29)$$

Table 2-1 lists a few values of α_{mn}.

m \ n	0	1	2
1	0.796	6.025	11.903
2	1.589	6.119	11.987
3	2.378	6.465	12.124

Table 2-1. A few values of α_{mn}.

In our annulus $a = 0.10$ m, so it is seen that α_{mn}/a is approximately 60 for m = 1. Similarly, L_z is 0.05 m, so $\frac{\pi}{L_z}$ is equal to 62.8, or nearly equal to α_{1n}/a. Therefore the frequencies of the first cross mode in either the z or r direction are approximately equal and have value in the vicinity of 3.3 - 3.6 kHz. Our primary interest is in frequencies corresponding to $L_{eff} = \lambda$, or $f = \frac{c}{L_{eff}} \cong 440$ Hz.

1. Uniform Cross Section Annular Resonator

a. Undriven case

As explained above, for low frequencies the annular resonator can be modeled as a straight pipe of length L_{eff} with periodic boundary conditions at the two end as shown in Fig. 2-2. Assume that there are two traveling waves in pipe. One is propagating in the positive x-direction and represented by

$$\mathrm{P}_+ = Ae^{j(\omega t - kx)}. \qquad (2.30)$$

The other propagates in the negative x- direction and given by

$$\mathrm{P}_- = Be^{j(\omega t + kx)}. \qquad (2.31)$$

The total pressure in the pipe is a sum of these two pressures and given by

$$P_t = P_+ + P_- = Ae^{j(\omega t - kx)} + Be^{j(\omega t + kx)}. \qquad (2.32)$$

These subscripts get used later in a different way use p and n for positive and negative instead of 1 and 2.

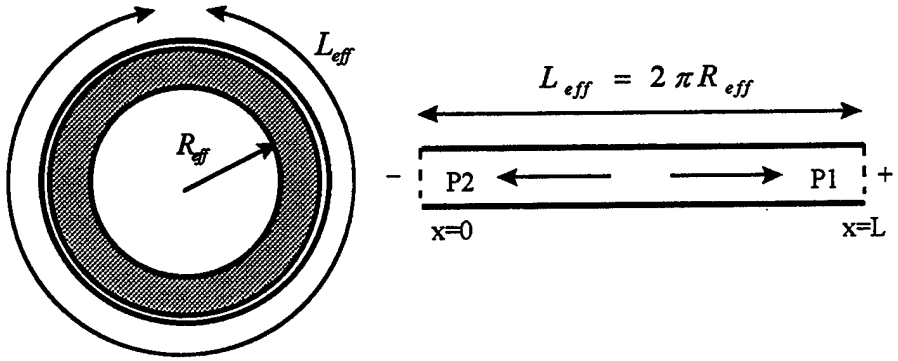

Figure 2-2. Annular resonator and equivalent straight resonator.

Also, the volume velocity U can be obtained from knowledge of the pressure and the pipe's acoustic impedance, $Z = \frac{\rho_o c}{S}$, where S is cross section area of pipe,

$$U_t = U_+ - U_- = \frac{Sk}{\omega \rho_o}\left[Ae^{j(\omega t - kx)} - B^{j(\omega t + kx)}\right]. \qquad (2.33)$$

Periodic boundary conditions are

$$P_{x=0} = P_{x=L} \qquad (2.34)$$

and

$$U_{x=0} = U_{x=L} \qquad (2.35)$$

where $L = L_{eff}$. Substituting Eq. (2.32) into (2.34) gives

$$A = B\frac{e^{jkL} - 1}{1 - e^{-jkL}}. \qquad (2.36)$$

Substituting this expression into Eq. (2.33) and applying Eq. (2.35) yields

$$\cos kL = 1. \qquad (2.37)$$

This implies that $kL = 2m\pi$ $(m = 0, 1, 2 \ldots\ldots)$, (2.38)

or $$f_m = \frac{mc}{L} . \tag{2.39}$$

It should be pointed out that L_{eff} has slightly different values for different values of m.

b. Driven case

In addition to knowing the resonance frequencies of the annular resonator, we are also interested in the mode shapes, i.e. the acoustic pressure and velocity as function of angular position. There is no unique orientation of the modes in an undriven, uniform cross section annulus. Either the system must be driven, or a nonuniformity in cross section must be introduced to fix the mode shapes. In the undriven uniform cross section case, any superposition of two degenerate orthogonal modes (one proportional to $\cos m\theta$, the other to $\sin m\theta$) satisfies the boundary conditions. In order to find the mode shape, it is necessary to install a driver in resonator. Assume that a branch driver is located at x = 0 as shown on Fig 2-3. The volume velocity injected by the driver is given by

$$U_D = u_D e^{j\omega t} . \tag{2.40}$$

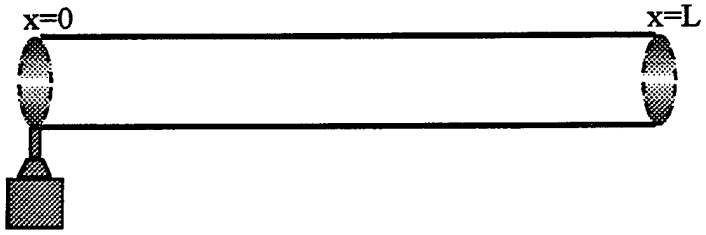

Figure 2-3. Driver installed straight resonator.

The boundary condition for pressure is given by

$$P_{x=0} = P_{x=L} \tag{2.41}$$

which is same as that for the undriven system. This conditions leads to

$$A\left(1-e^{-jkL}\right)+B\left(1-e^{jkL}\right)=0. \tag{2.42}$$

The boundary condition for volume velocity now includes an additional term and is given by

$$U_{x=0} = U_{x=L} + U_D, \tag{2.43}$$

which yields the equation

$$\mathrm{A}\left(1 - e^{-jkL}\right) - \mathrm{B}\left(1 + e^{jkL}\right) = \frac{\rho_o c}{S} u_D. \tag{2.44}$$

Equations. (2.42) and (2.44) can be expressed in matrix form as

$$\begin{bmatrix} 1 - e^{-jkL} & 1 - e^{jkL} \\ 1 - e^{-jkL} & -1 + e^{jkL} \end{bmatrix} \begin{bmatrix} \mathrm{A} \\ \mathrm{B} \end{bmatrix} = \begin{bmatrix} 0 \\ \frac{\rho_o c}{S} u_D \end{bmatrix}. \tag{2.45}$$

This equation has the form $MC = U$. The value of the coefficients A , B can be determined from $C = M^{-1}U$. Once A and B are known, the pressure and volume velocity are found from Eqs. (2.32) and (2.33).

2. Constricted Annular Resonator.

a. Frequency vs area ratio (no driver)

The analysis of the constricted resonator is more complicated due to its non uniform cross sectional area. The geometry is shown in Fig. 2-4.

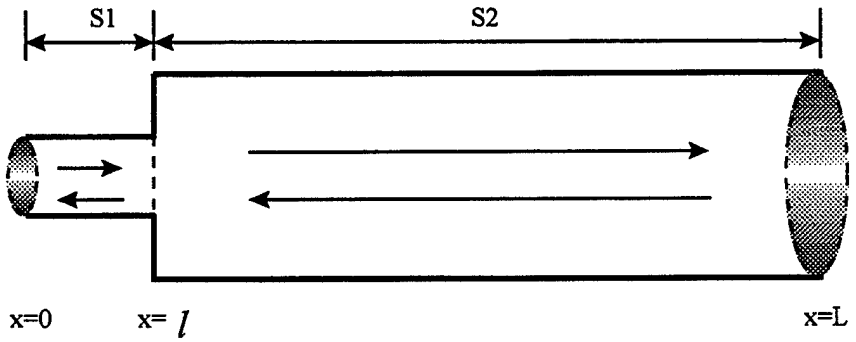

Figure 2-4. Constricted resonator with no driver.

Calculation of the resonance frequency of a constricted resonator is similar to that of the uniform cross section resonator. In order to solve this case, the basic equations

of pressure and volume velocity in each section have same form as the uniform cross section resonator .

$$\mathrm{P}_1 = Ae^{j(\omega t - k_1 x)} + Be^{j(\omega t + k_1 x)}, \tag{2.46}$$

$$\mathrm{P}_2 = Ce^{j(\omega t - k_2 x)} + De^{j(\omega t + k_2 x)}. \tag{2.47}$$

At the junction of two sections, pressure and volume velocity are continuous which gives the following equations

$$\mathrm{P}_1(x = l) = \mathrm{P}_2(x = l), \tag{2.48}$$

$$\mathrm{P}_1(x = 0) = \mathrm{P}_2(x = L), \tag{2.49}$$

$$U_1(x = l) = U_2(x = l), \tag{2.50}$$

$$U_1(x = 0) = U_2(x = L). \tag{2.51}$$

These equations can be combined into a 4 × 4 matrix in the following form.

$$\begin{bmatrix} e^{-jk_1 l} & e^{jk_1 l} & -e^{-jk_2 l} & -e^{jk_2 l} \\ 1 & 1 & -e^{-jk_2 L} & -e^{jk_2 L} \\ e^{-jk_1 l} & -e^{jk_1 l} & \frac{-S_2 k_2}{S_1 k_1} e^{-jk_2 l} & \frac{S_2 k_2}{S_1 k_1} e^{jk_2 l} \\ 1 & -1 & \frac{-S_2 k_2}{S_1 k_1} e^{-jk_2 L} & \frac{S_2 k_2}{S_1 k_1} e^{jk_2 L} \end{bmatrix} \begin{bmatrix} \mathrm{A} \\ \mathrm{B} \\ C \\ D \end{bmatrix} = 0. \tag{2.52}$$

This matrix has the form of $MC = 0$. The resonance frequencies are those frequencies that satisfy the equation det[M] = 0.

Unlike the uniform cross section case, the introduction of a constriction splits the degeneracy of the modes. The two modes, called the high frequency and low frequency modes, correspond to different mode shapes. (In what follows, the word "frequency" be will frequency dropped and the modes referred to, simply, as "high" and "low".) The high mode has a pressure antinode centered on the constriction whereas the low mode has a velocity antinode centered on the constriction. The difference in frequency between the high and low mode increases with increasing length or decreasing cross sectional area of the constriction.

The dependence of the frequency splitting is shown in Figs. 2.5 a-c. The plots show resonance frequency as a function of area ratio for three different constriction lengths. The resonator contains air at 20°C and atmosphere pressure. Area ratio is defined as the ratio of the cross sectional (open) area in the constriction to that of the resonator. In the limits of zero area ratio, i.e. when the constriction is completely blocked, the high mode frequency corresponds to $\lambda = (L_{eff} - L_{constriction})$ and the low mode frequency corresponds to $\lambda = 2(L_{eff} - L_{constriction})$. These limits are appropriate for the two lowest modes of a rigid, rigid resonator of length $L_{eff} - L_{constriction}$.

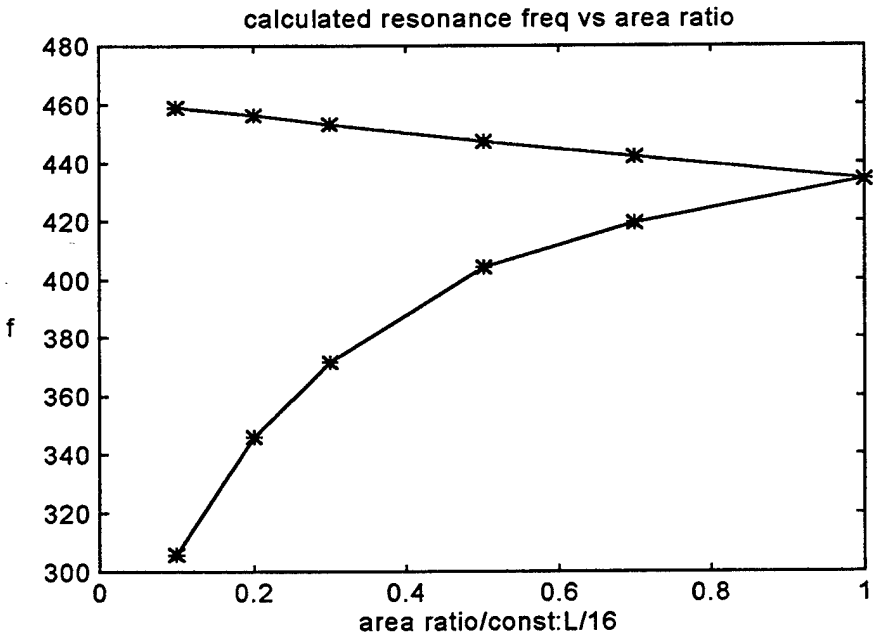

Figure 2-5a. Resonance frequencies with a long constriction $\left(\frac{L_{eff}}{16}\right)$

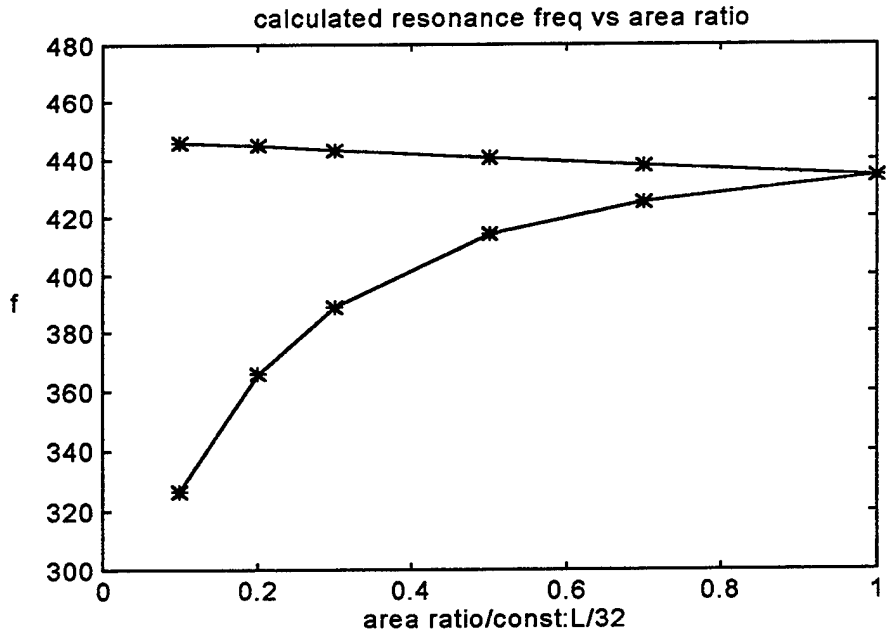

Figure 2-5b. Resonance frequencies with a medium length constriction $\left(\frac{L_{eff}}{32}\right)$

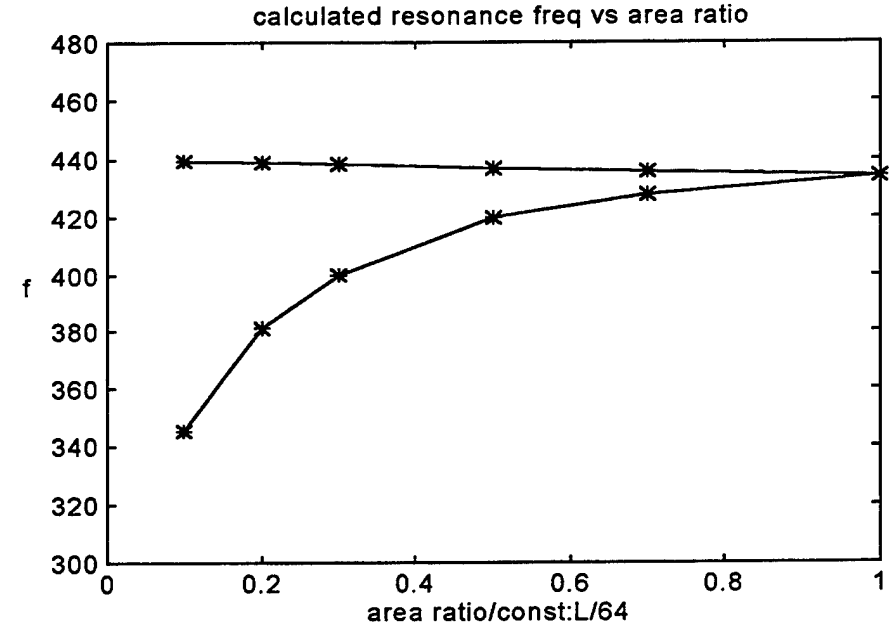

Figure 2-5c. Resonance frequencies with a short constriction $\left(\frac{L_{eff}}{64}\right)$

b. Mode shapes of a constricted resonator

Calculation of the pressure distribution in a driven, constricted resonator is also similar to that for the driven uniform cross section case. For the driven, constricted resonator, the resonator is divided into three sections, as shown in Fig. 2-6. The driver is located at x = d.

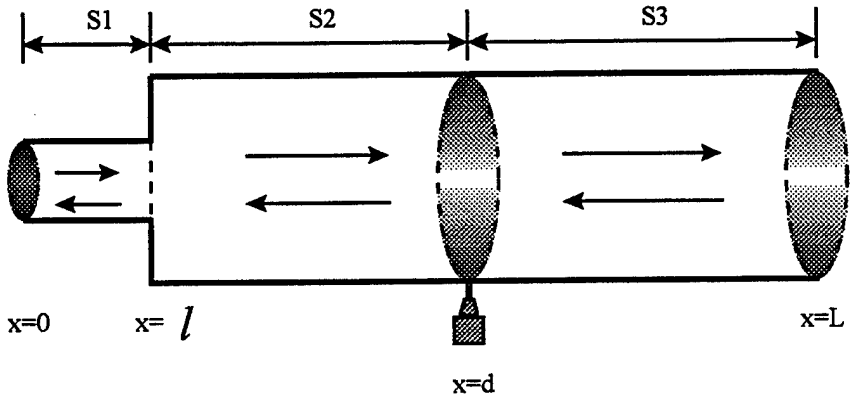

Figure 2-6. Constricted resonator with driver.

This system gives rise to the following set of equations for pressure and volume velocity in the three regions:

$$P_1 = Ae^{j(\omega t - k_1 x)} + Be^{j(\omega t + k_1 x)}, \tag{2.53}$$

$$P_2 = Ce^{j(\omega t - k_2 x)} + De^{j(\omega t + k_2 x)}, \tag{2.54}$$

$$P_3 = Ee^{j(\omega t - k_2 x)} + Fe^{j(\omega t + k_2 x)}, \tag{2.55}$$

$$U_1 = \frac{S_1 k_1}{\omega \rho_o} Ae^{j(\omega t - k_1 x)} - \frac{S_1 k_1}{\omega \rho_o} Be^{j(\omega t + k_1 x)}, \tag{2.56}$$

$$U_2 = \frac{S_2 k_2}{\omega \rho_o} Ce^{j(\omega t - k_2 x)} - \frac{S_2 k_2}{\omega \rho_o} De^{j(\omega t + k_2 x)}, \tag{2.57}$$

$$U_3 = \frac{S_2 k_2}{\omega \rho_o} Ee^{j(\omega t - k_2 x)} - \frac{S_2 k_2}{\omega \rho_o} Fe^{j(\omega t + k_2 x)}, \tag{2.58}$$

and

$$U_D = u_D e^{j\omega t}. \tag{2.59}$$

The three different sections also give rise to six boundary conditions:

$$P_1(x=0) = P_3(x=L), \tag{2.60}$$

$$U_1(x=0) = U_3(x=L), \tag{2.61}$$

$$P_1(x=l) = P_2(x=l), \tag{2.62}$$

$$U_1(x=l) = U_2(x=l), \tag{2.63}$$

$$P_2(x=d) = P_3(x=d), \tag{2.64}$$

and

$$U_2(x=d) + u_D = U_3(x=d). \tag{2.65}$$

Application of these boundary conditions to Eqs. (2.53) - (2.59) yields a set of equations which can be combined into a matrix equation of the form $MC = U$.

$$\begin{bmatrix} 1 & 1 & 0 & 0 & -e^{-jk_2L} & -e^{jk_2L} \\ 1 & -1 & 0 & 0 & \frac{-S_2k_2}{S_1k_1}e^{-jk_2L} & \frac{S_2k_2}{S_1k_1}e^{jk_2L} \\ e^{-jk_1l} & e^{jk_1l} & -e^{-jk_2l} & -e^{jk_2l} & 0 & 0 \\ e^{-jk_1l} & -e^{jk_1l} & \frac{-S_2k_2}{S_1k_1}e^{-jk_2l} & \frac{S_2k_2}{S_1k_1}e^{jk_2l} & 0 & 0 \\ 0 & 0 & e^{-jk_2d} & e^{jk_2d} & -e^{-jk_2d} & -e^{jk_2d} \\ 0 & 0 & e^{-jk_2d} & -e^{jk_2d} & -e^{jk_2d} & e^{jk_2d} \end{bmatrix} \begin{bmatrix} A \\ B \\ C \\ D \\ E \\ F \end{bmatrix} = \begin{bmatrix} 0 \\ 0 \\ 0 \\ 0 \\ 0 \\ \frac{-\rho_o c}{S_2}u_D \end{bmatrix} \tag{2.66}$$

Solving the inverse form of Eq. (2.66) gives the value of the coefficients A through F. Substitution of these coefficients into Eq. (2.53)-(2.55) gives the mode shapes.

(1) Mode Selection and Driver Location. Because of dissipation, the quality factor (Q) of a particular mode is finite. This means that, in general, when the resonator is driven at a frequency in the vicinity of the resonance of either the high or low mode, both modes will be excited. In order to measure the mode shape of a single mode, it is necessary to excite only that mode as nearly as possible. This can be accomplished to an acceptable degree by proper location of the driver. If the driver is positioned at a pressure antinode of a particular mode and driven at the resonance frequency of that mode, then that mode is the predominant one excited.

Mode selection is illustrated the next sequence of figures which show the calculated frequency response and mode shapes for the resonator with a constriction

length of $\frac{L_{eff}}{32}$ and area ratio 0.7. For Fig. 2-7, the driver is located 180° from the center of the constriction which should correspond to a pressure antinode for the high mode. Figure 2-7a shows the frequency response as indicated by computed magnitude of acoustic pressure measured 45° from constriction. This figure shows that there is only a single peak in the frequency response. The peak frequency, 439.0 Hz, corresponds to the resonance frequency of the high mode for a $\frac{L_{eff}}{32}$ long constriction with a 0.7 area ratio, as shown in Fig. 2-5b. Figure 2-7b shows the calculated mode shape when the resonator is driven at 439.0 Hz. It is seen that there is indeed a pressure anitnode at both the constriction and driver location. It is also evident that the standing wave ratio is very high, another indication of single-mode excitation.

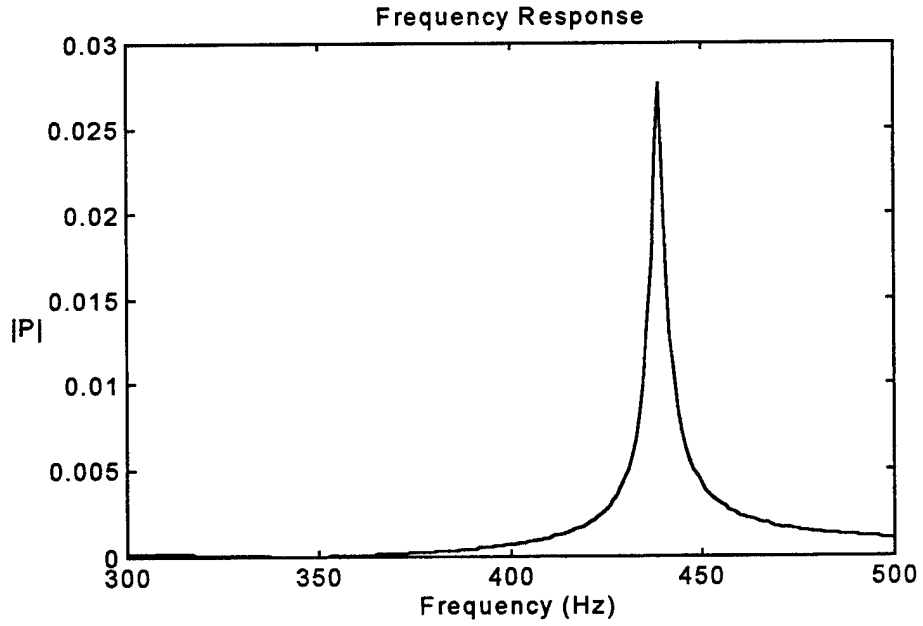

Figure 2-7a. Frequency response of the constricted resonator when driver is located 180° from the constriction and driven at the high mode resonance frequency for the $\frac{L_{eff}}{32}$ length, 0.7 area ratio constriction.

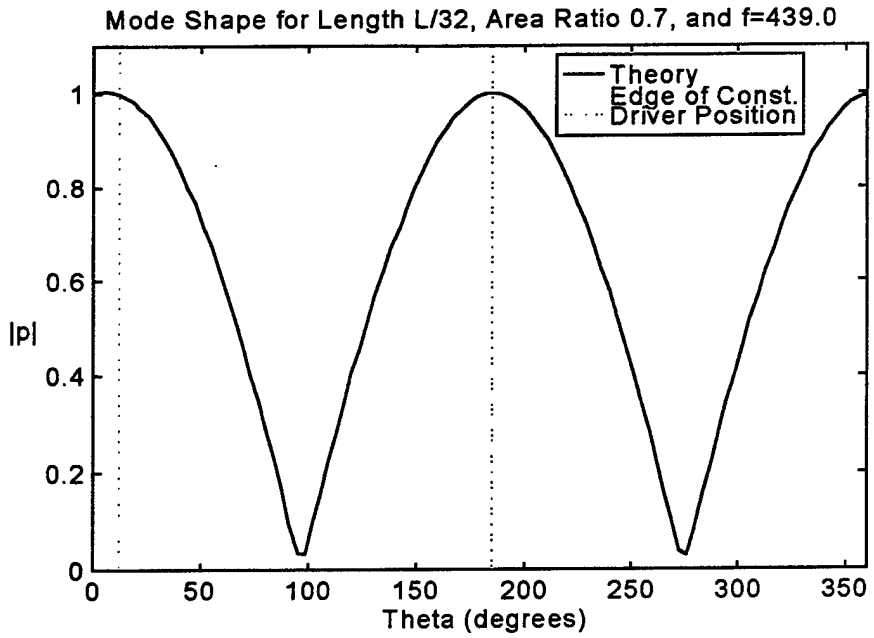

Figure 2-7b. Mode shape when the resonator is driven at the peak frequency as determined from Fig. 2-7a.

Figure 2-8a shows the frequency response when the driver is moved to a location 90° from the constriction. This driver location should be near a pressure node for the high mode and pressure antinode for the low mode. The frequency response again shows only one peak. Comparison with Fig. 2-5b indicates that this mode is the low mode. Figure 2-8b shows the mode shape. It is seen that now there is a pressure node at the constriction. Again, the standing wave ratio is high indicating single-mode excitation.

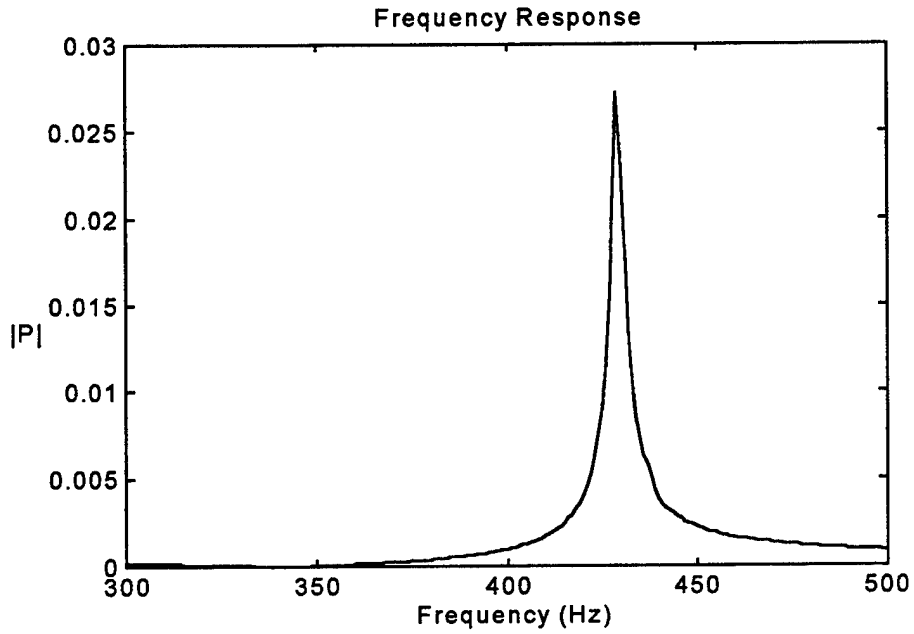

Figure 2-8a. Frequency response of the constricted resonator when driver is located 90° from the constriction and driven at the low mode resonance frequency for the $\frac{L_{eff}}{32}$ length, 0.7 area ratio constriction.

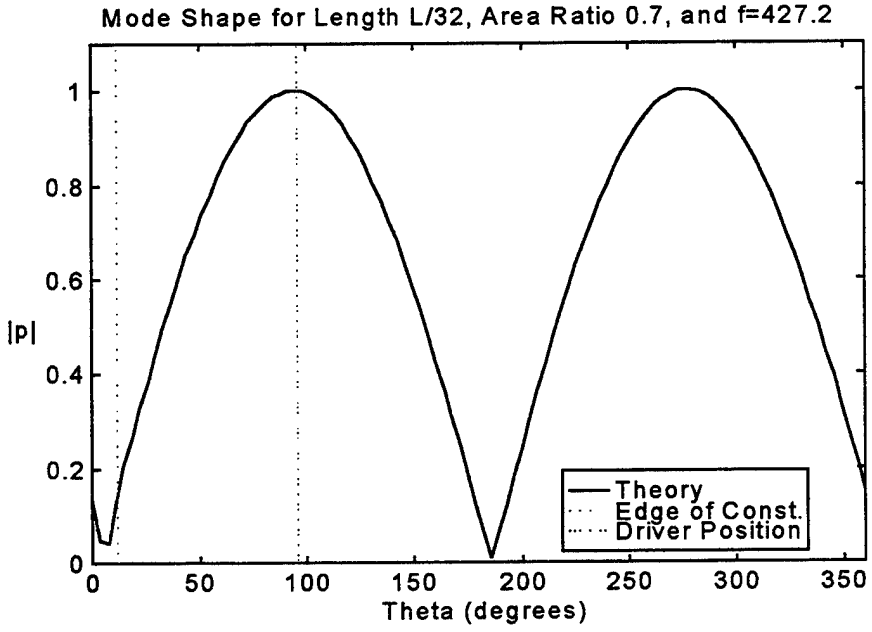

Figure 2-8b. Mode shape when the resonator is driven at the peak frequency as determined from Fig. 2-8a.

In the cases of the driver located at 180 degrees or 90 degrees from the constriction, the driver excites only one mode, either high or low. If the driver is placed at a position other than 180 degree or 90 degree, two modes will be excited simultaneously. Figure 2-9 shows the frequency response when the driver is located 45 degrees from the constriction. We have used the $L_{eff}/16$, 0.1 area ratio constriction to make the amount of frequency splitting larger.

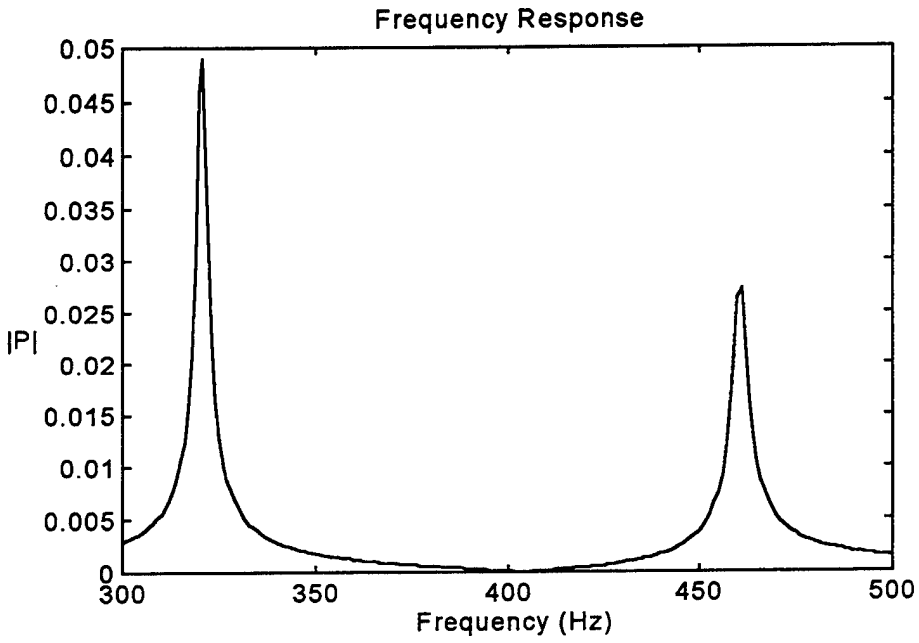

Figure 2-9a. Frequency response when driver is located 45° from the $L_{eff}/16$, 0.1 area ratio constriction.

We can see from Fig. 2-9a that both the high and low modes are excited. In this case, they are well separated, in other words, there is no significant overlap. When there is little overlap, it is easy to pick up the resonance frequency of each mode. A constriction of small area ratio (0.1) and long size ($L_{eff}/16$, 22.5 degree), as in Fig. 2-9a, separates the two modes well enough for there to be little overlap. Figure 2.9b shows the mode shape when the resonator is driver at the lower peak frequency. This figure shows

that even when the driver is at a location which would allow both modes to be excited, when the modes are well separated, single mode excitation is still possible.

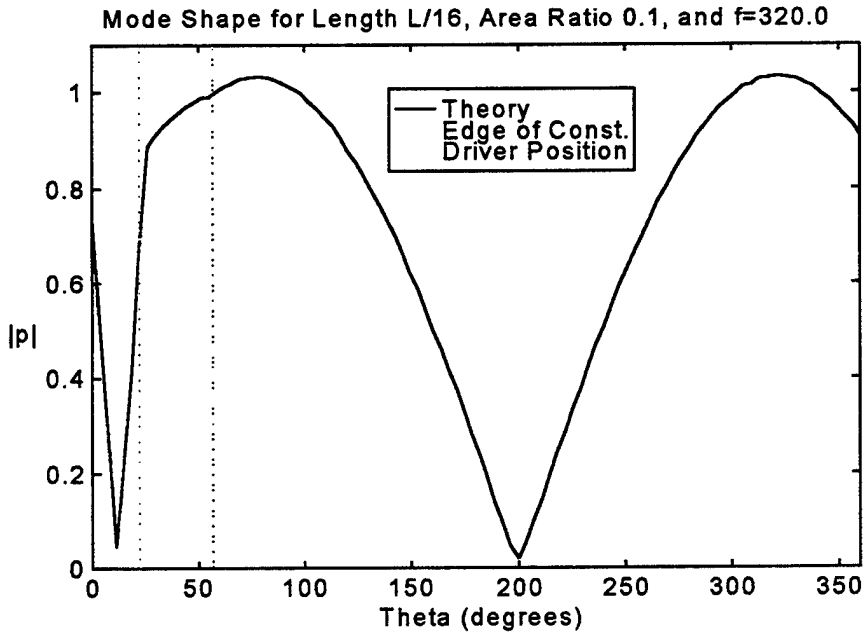

Figure 2-9b. Mode shape when the resonator is driven at the lower of the two peak frequencies from Fig. 2-9a.

Figure 2-10a shows the frequency response for the $L_{eff}/32$ length, 0.7 area ratio constriction used in earlier figures. In contrast to Fig. 2-9a, the modes show significant overlap. This overlap causes two problems. First, it means that a driver located at 45° will excite both modes to a significant degree, even when driver at one of the peak frequencies. Second, the peak frequencies no longer correspond to the resonance frequencies. Overlapping is most significant for large area ratio, short constrictions.

Figure 2-10b shows the mode shape when the resonator is driven at the lower peak frequency in Fig. 2-10a. It is seen that the standing ratio is low in this case, indicating excitation of more than one mode. The next section addresses a technique to determine resonance frequencies in the case of significant overlap.

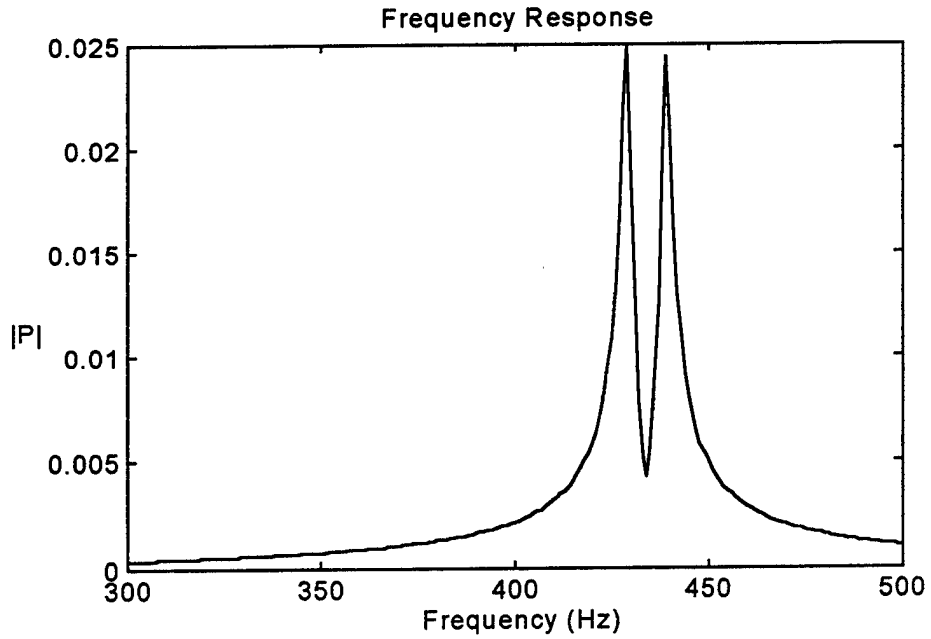

Figure 2-10a. Overlapped wave form of frequency response with driver 45 degrees from a constriction which has a 0.7 area ratio and $L_{eff}/64$, (5.625 degree) length.

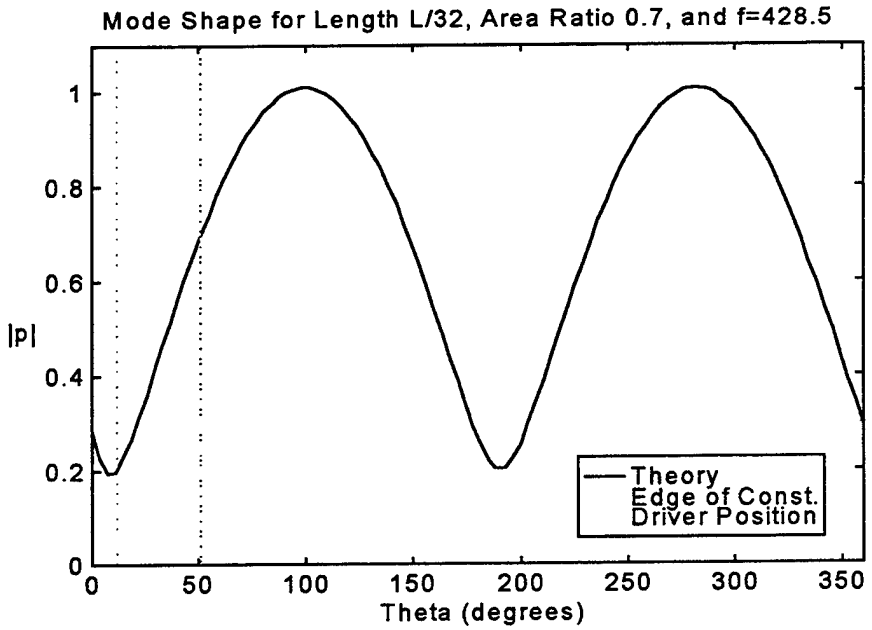

Figure 2-10b. Mode shape when the resonator is excited at the lower peak frequency in Fig 2-10a.

D. POLE - ZERO ANALYSIS

For understanding the acoustics of an annular resonator, it is important to find accurate values of the resonance frequencies. These resonance frequencies are independent of the driver location but are dependent upon what kind of constriction is being used - the length and area ratio. As we have seen, the driver may excite one or two modes simultaneously depending upon its excitation frequency and location. When only one mode is excited, it is simple to find resonance frequency by finding the frequency corresponding to the peak in the frequency response . But for the case when the driver excites two modes simultaneously, the peak frequency cannot be used to determine the resonance frequency. This situation was discussed in the previous section. Pole-zero analysis can be used to determine the resonance frequencies in the case of significant modal overlap.

1. Analysis

For a driven simple harmonic oscillator, the complex speed is represented by [Ref 1]

$$\vec{u} = \frac{F e^{j\omega t}}{R_m + j\left(\omega m - \frac{s}{\omega}\right)}. \qquad (2.67)$$

The expression for $\vec{u}$ can be written as

$$\vec{u} = \frac{-j\omega \frac{F}{m} e^{j\omega t}}{\omega^2 - j\frac{\omega_o}{Q}\omega - \omega_o^2} \qquad (2.68)$$

by introducing the resonance frequency ω_o and quality factor, $Q = {\omega_o m}/{R_m}$.

By analogy, we assume the pressure in a resonator driven near resonance, at one point in space, has the form

$$P = \frac{A}{\omega^2 - j\frac{\omega_o}{Q}\omega - \omega_o^2} \tag{2.69}$$

where Q is now the quality factor for the resonator. Factoring the denominator of Eq. (2.69) results in

$$P = \frac{A}{\left[\omega - \left(j\frac{\omega_o}{2Q} + \sqrt{\omega_o^2 - \left(\frac{\omega_o}{2Q}\right)^2}\right)\right]\left[\omega - \left(j\frac{\omega_o}{2Q} - \sqrt{\omega_o^2 - \left(\frac{\omega_o}{2Q}\right)^2}\right)\right]}. \tag{2.70}$$

This equation can be simplified if the denominator is written as [Ref 2]

$$(\omega + jp_1)(\omega + jp_2), \tag{2.71}$$

where the poles p_1 and p_2 are,

$$p_1 = -\frac{\omega_1}{2Q_1} + j\sqrt{\omega_1^2 - \left(\frac{\omega_1}{2Q_1}\right)^2} \tag{2.72}$$

and

$$p_2 = -\frac{\omega_1}{2Q_1} - j\sqrt{\omega_1^2 - \left(\frac{\omega_1}{2Q_1}\right)^2}, \tag{2.73}$$

or

$$p = -\frac{\omega_1}{2Q_1} \pm j\sqrt{\omega_1^2 - \left(\frac{\omega_1}{2Q_1}\right)^2} \tag{2.74}$$

where $\omega_1 = \omega_o$, for the single mode case. The poles are written in the form $(\omega + jp)$ because the Hewlett Packard signal analyzer used for experimental measurement outputs the poles in that form. Equation (2.74) can be simplified into a form given by

$$p = -a \pm jb \quad \text{where} \quad a = \frac{\omega_1}{2Q_1} \quad \text{and} \quad b = \sqrt{\omega_1^2 - \left(\frac{\omega_1}{2Q_1}\right)^2}. \tag{2.75}$$

For two overlapping modes, the complex pressure amplitude is the sum of the individual amplitudes

$$P_{tot} = P_1 + P_2 \tag{2.76}$$

and P_{tot} has the form

$$P_{tot} = \frac{A_1(\omega + jp_3)(\omega + jp_4) + A_2(\omega + jp_1)(\omega + jp_2)}{(\omega + jp_1)\cdots\cdots(\omega + jp_4)}. \tag{2.77}$$

So, even though the two modes are overlapped and the amplitude of the individual responses are added, the poles still show separable frequencies.

The numerator of Eq. (2.77) can be factored in the same way as the denominator of Eq. (2.69). In this case the numerator is

$$\left[\omega + \left(\frac{-jc + d}{2(A_1 + A_2)}\right)\right]\left[\omega + \left(\frac{-jc - d}{2(A_1 + A_2)}\right)\right], \tag{2.78}$$

where

$$c = A_1(-\frac{\omega_2}{Q_2}) + A_2(-\frac{\omega_1}{Q_1}), \tag{2.79}$$

and

$$d = \sqrt{-\left[A_1\left(\frac{-\omega_2}{Q_2}\right) + A_2\left(\frac{-\omega_1}{Q_1}\right)\right]^2 + 4(A_1 + A_2)(A_1\omega_1^2 + A_2\omega_1^2)}. \tag{2.80}$$

From Eq. (2.78) we can find zeros.

The resonance frequency and quality factor can be obtained from the poles using Eq. (2.75). The resonance frequency is then

$$\omega_1 = \sqrt{a^2 + b^2} \tag{2.81}$$

and the quality factor is

$$Q_1 = \frac{\omega_1}{2a}. \tag{2.82}$$

If Q is large, an approximation can be used to simplify Eq. (2.81). The term of $\frac{\omega_1}{2Q_1}$ can be neglected since $\left(\frac{\omega_1}{2Q_1}\right)^2$ is small compared to ω_1^2. So, $b \cong \omega_1$.

For data analysis, we fit the measured frequency response using pole-zero analysis. The fit parameters give the resonance frequency and Q of the individual modes.

E. THERMO-VISCOUS DAMPING

Up to this point, losses have been ignored. However any real gas has viscosity and will exchange heat with the walls of the resonator. The boundary condition at the walls of the resonator is that the normal velocity is zero. When viscosity is included the correct boundary condition has both the normal and tangential velocity going to zero. This creates a viscous boundary layer which contributes viscous losses to the propagation of sound [Ref. 3,4]. Similarly, the gas near the walls will exchange heat with the walls. This thermal boundary layer also contributes losses to the sound propagation [Ref. 3,4]. While these viscous and thermal effects are complicated, if the boundary layer thicknesses are small compared to the cross sectional dimensions of the resonator, the effects can be included by a modification of the wave number k.

The frequency dependent viscous and thermal boundary layer thickness δ_v and δ_K are given by

$$\delta_v = \sqrt{\frac{2\mu}{\omega\rho}} \tag{2.83}$$

and

$$\delta_K = \sqrt{\frac{2K}{\omega \rho c_p}} \tag{2.84}$$

where μ is the viscosity, K is the thermal conductivity, c_p is the specific heat and ρ is the density of the gas. The wave number k is then given by [Ref. 5]

$$\mathrm{k} = \frac{\omega}{c}\sqrt{\frac{2r_h + (\gamma - 1)\delta_K(1+j)}{2r_h - \delta_v(1+j)}} \tag{2.85}$$

where r_h is the hydraulic radius, which is the ratio of the cross sectional area to the perimeter. It should be noted that since the hydraulic radius is different in the constriction and in the main channel, and that k is now complex. The imaginary part of k is related to the thermo-viscous damping.

F. END EFFECTS

In the earlier analysis, the boundary conditions used at the ends of the constriction were continuity of pressure and volume velocity. Using only plane wave analysis, the pressure and particle velocity are constant across the cross section. However, at the constriction end, the velocity and pressure have a spatial dependence and thus the plane wave theory is not as accurate near the ends as it is away from them.

The spatial variation in the pressure can be described using non-propagating higher order modes. These non-propagating modes store energy near the constriction ends. Their effect on the plane wave propagation can be modeled as a lumped impedance element. [Ref. 6]. The lumped impedance can be obtained from a variety of methods. A first approximation involves modeling the impedance as an added mass much like the end correction for radiation at the end of a tube. This added mass can be computed using conformal mapping. [Ref. 6]. A more accurate method involves including higher order modes near the constriction end. [Ref. 7]. While computationally more intensive than the conformal mapping solution, the higher order mode solution is more accurate.

After computing the lumped impedance $\mathrm{Z}(\omega)$, the boundary condition for the pressure becomes (the volume velocity boundary condition is unchanged.)

$$\mathrm{P}_1(l) = \mathrm{P}_2(l) + \mathrm{Z}(\omega)U_2(l) \tag{2.86}$$

where P_1 is the pressure in unconstricted region and P_2 is the pressure in constriction. U_2 is the velocity in the constriction. The constriction is at $x = l$.

III. EXPERIMENTAL APPARATUS AND PROCEDURE

A. INTRODUCTION

A description of the experimental apparatus and the procedures for data acquisition are presented in this chapter. The first section will include a description of the annular resonator, constrictions, the driver, the microphone and electronic instrumentation. The second section discusses the data acquisition system. The third section is a detailed discussion of the experimental procedure.

B. EXPERIMENTAL APPARATUS

1. Resonator and Driver

Figure 3-1 is an illustration of the annular resonator and acoustic driver. The sides and bottom of resonator are made of aluminum. The top of resonator is made of plexiglas to allow visual sighting of the relative positioning of the constriction and the driver. More details about each part will follow.

The dimensions of the resonator were chosen to give longitudinal resonance frequencies in the 300 ~ 500 Hz range and to be well below the cutoff frequency for cross modes. The resonator consists of two main parts as shown on Fig. 3-1. One piece is an aluminum ring with 15.30±0.02 cm inner radius and 1cm thick wall. This ring formed the outer side wall of the resonator. The other piece is a solid aluminum cylinder which is concentric with the outer ring. The inner radius of resonator is 10.0±0.01 cm. The height of resonator is 5.0±0.01 cm. The resonator is capped on the open side with 1cm thick plexiglas plate with a radius of 16.0 cm. The bottom plate of the resonator is made of aluminum and its thickness is 1.0 cm. Sixteen microphones are installed in the cap to measure the spatial acoustic pressure distribution inside resonator. The installation of microphones will be discussed later.

The cap is bolted with 10.7 cm long threaded rod in the center and 8 clamp bars as shown on Fig. 3-2. To ensure a tight seal (for a high quality factor), vacuum grease was applied to the surface of the aluminum ring and center piece.

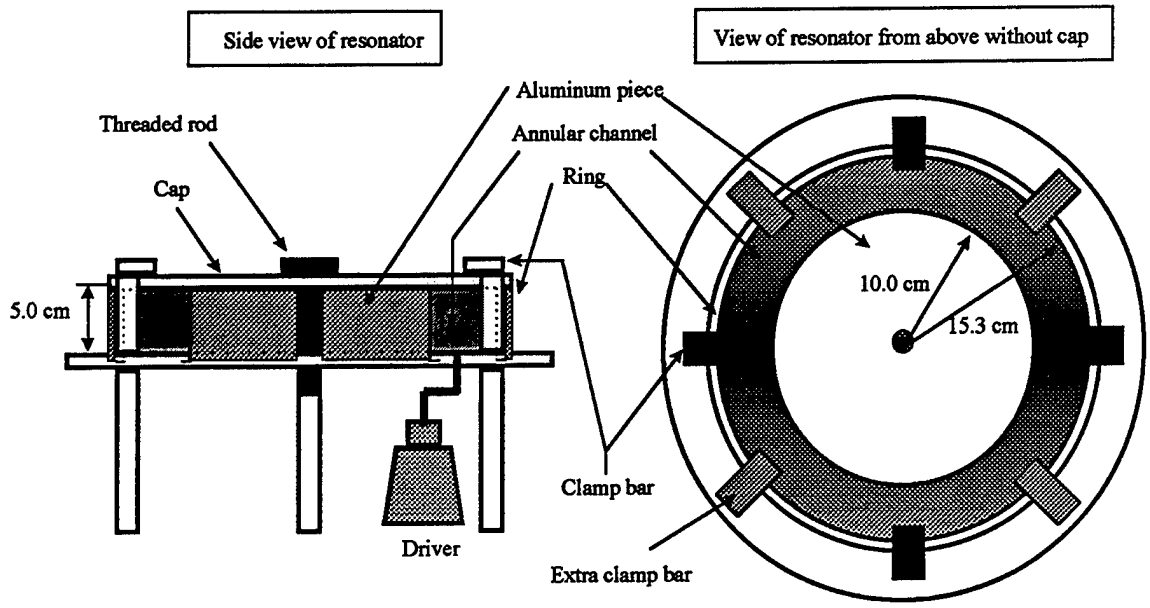

Figure 3-1. Illustration of resonator and driver.

The acoustic signal was generated by a 40 W , 16 ohm external driver. The driver was connected to the resonator by a 3.5 cm long piece of plastic hose with 0.4 cm diameter. The driver was excited by the output of a Hewlett Packard 3562A dynamic signal analyzer sent through a Techron 5507 power amplifier. The signal analyzer was used to determine the frequency response of the resonator. Typically, the resonator was driven with random noise with a 1 Vrms source level. To measure the mode shape, a Hewlett Packard 33120A function generator was used to excite the resonator at the resonance frequency determined from the built-in pole-zero analysis of the frequency response using the signal analyzer.

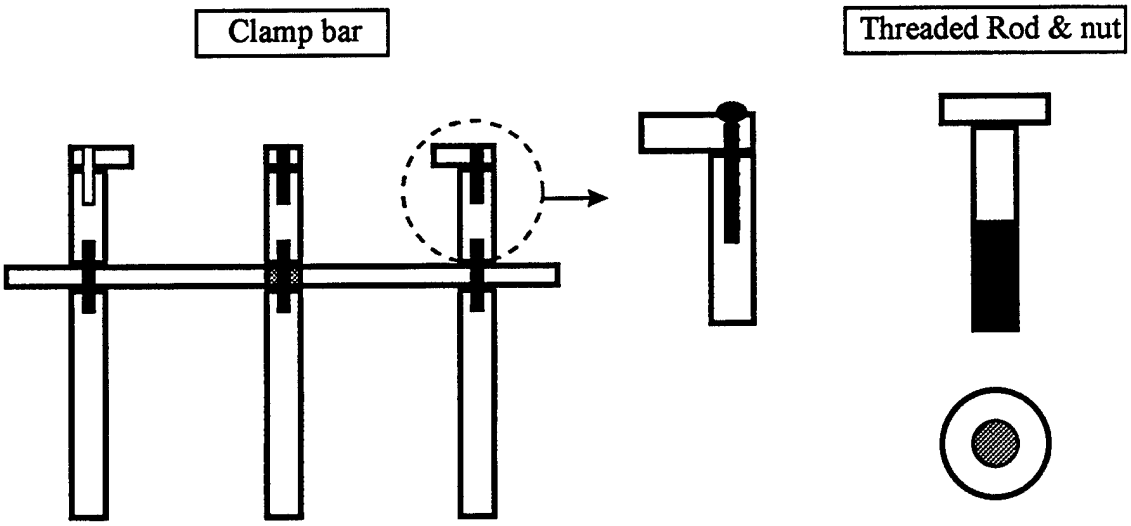

Figure 3-2. Illustration of clamp bar, threaded rod and nut.

2. Microphones

For the experiment, 16 Panasonic WM60-AY microphones were used to measure the pressure distribution inside resonator. The dimensions of the microphones are 6 mm in height and 5mm in diameter. The sensitivity is -42 dB ± 3dB re 1Pa. A Hewlett Packard 6237B triple output power supplier provided 9 V DC to each microphone.

a. Installation of microphones

The microphones were installed as shown on Fig. 3-3. The first intention was to use only one microphone and rotate the cap for each different position to measure the mode shape. However, the rotation of cap broke the sealing between the plexiglas cap and aluminum bodies of the resonator making the measurements very time consuming and nonrepeatable.

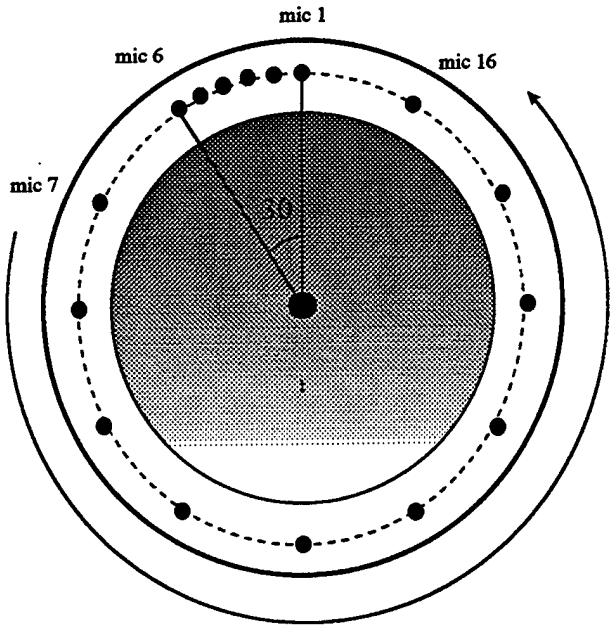

Figure 3-3. Installation of 16 microphones on the plexiglas cap.

We decided to install 16 microphones in order to protect sealing and reduce the time required for data acquisition. For the precise measurement in constricted area, 6 microphones are located in first 30 degree region where a constriction is located. The remaining 10 microphones are located 30 degrees apart. The microphones were installed in the center of the annular channel. To install the microphones, 16 holes were drilled part way through the plexiglas cap. These holes were slightly larger than the diameter of the microphone. A smaller hole was drilled concentric with each of the larger holes. This smaller hole penetrated the cap. Therefore the hole size presented to the inside of the resonator was much smaller than the microphone diameter. The small hole diameter is 0.15 cm. The microphones were sealed into the holes with silicon glue. The error in the microphone position is estimated to be less than $\pm$ 0.25°.

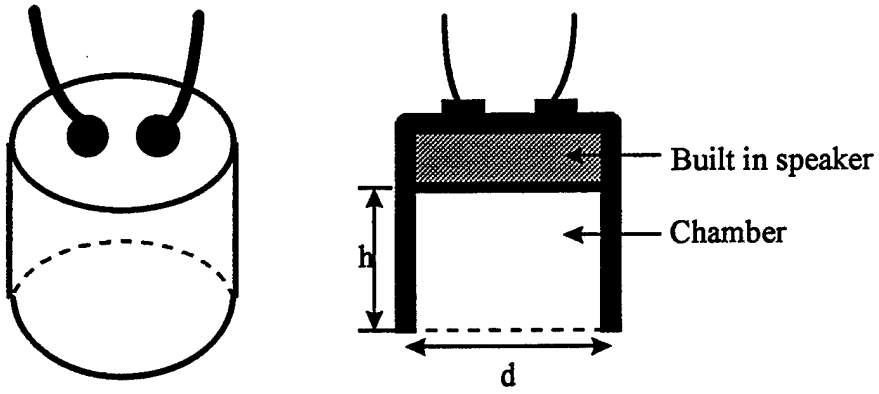

Figure 3-4 . Chamber used for microphone calibration

b. Calibration of microphones

Because 16 microphones are used for sensing the pressure distribution, the first step was to calibrate all the microphones over the 300 ~ 500 Hz frequency range interest. For the calibration, a custom made chamber with a built in speaker was used. As shown on Fig. 3-4, the diameter of the chamber is 3.0 cm and the height is 2.50 cm. At first we tried to measure the pressure for each microphone at the same position relative to the driver in an otherwise empty resonator. However, the phase shift caused by the resonators' resonance made calibration very sensitive to small errors in position. Instead, the top cap has removed and the calibration chamber was positioned directly over each microphone. The frequency response was measured for each microphone over a 300 ~ 500 Hz range. A typical frequency response is shown in Fig. 3-5. This sweeping and data storage were done by Hewlett Packard 35665A dynamic signal analyzer. For the calibration, the signal analyzer was set to swept sine mode with a settling time of 20 cycles and integration time of 50 cycles. The chamber was placed onto the cap where each microphone is located and the chamber was sealed on the cap with vacuum grease.

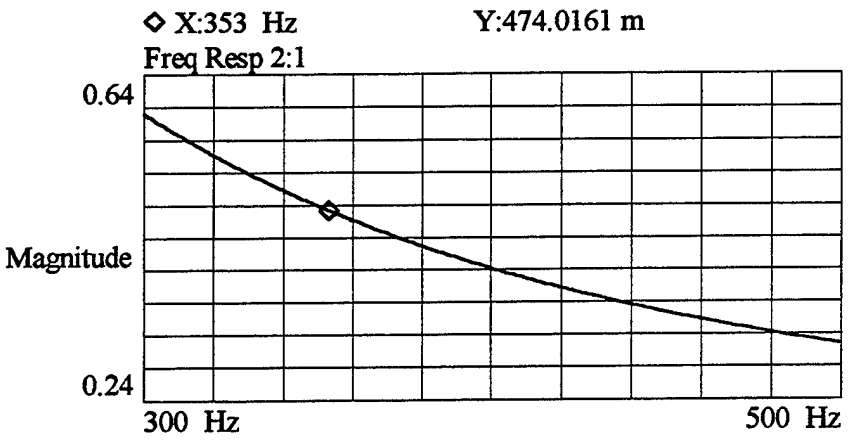

Figure 3-5. Frequency response of Mic. #1 covered by the calibration chamber.

Microphone #1 was used as the reference for comparison calibrations of the other 15 microphones. Each microphone's output was divided by that of microphone #1 to create a correction factor as shown on Fig. 3-6. When measuring the mode shape, the output from each microphone was divided by the appropriate correction factor to obtain the corrected amplitude at a particular location and driving frequency. For example, consider the case when the measured amplitude from microphone # 12 is 50 mV at 455 Hz. The correction factor is 0.739 from the Fig. 3-6. Dividing 50 mV by 0.739 gives 67.66 mV as the corrected measurement. Generally, the correction factors were between 0.7 and 1.2.

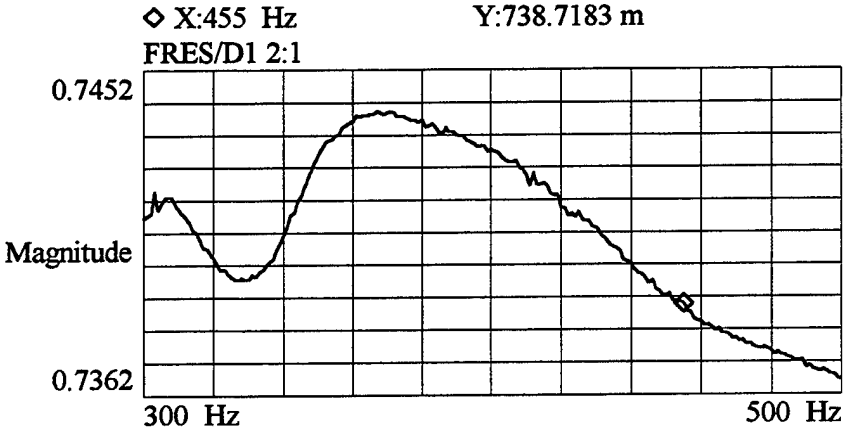

Figure 3-6. Plot of correction factor for Mic. #12 referenced to Mic. #1. The correction factor is 0.739 at 455 Hz.

3. Constriction

To explore a wide range of parameters, various sizes of constriction are necessary. When considering the material selection for this constriction, a couple of factors came to mind. The material had to be rigid and have good machining propertied for ease of fabrication. These two factors led to the selection of PVC (Polyvinylchloride). Figure 3-7 shows the design along with the nominal and measured dimensions for the various constrictions used. For the experiment, 3 different angular widths were used. The width of constriction is given by the θ shown in Fig. 3-7. The three widths are 22.5° , 11.25° and 5.625°. The 22.5° constriction corresponds to $\frac{1}{16}$ of the effective circumference of the resonator. 11.25° corresponds to $\frac{1}{32}$ of L_{eff} and 5.625° corresponds to $\frac{1}{64}$ of L_{eff}. The area ratio is the ratio of open area in the constriction (which is the shaded black square in Fig. 3-7) to cross sectional area of resonator. In Fig 3-7, S1 stands for the open area and S2 stands for the open cross sectional area of the constriction. The table in Fig. 3-7 gives the geometrical parameters of 32 different constrictions.

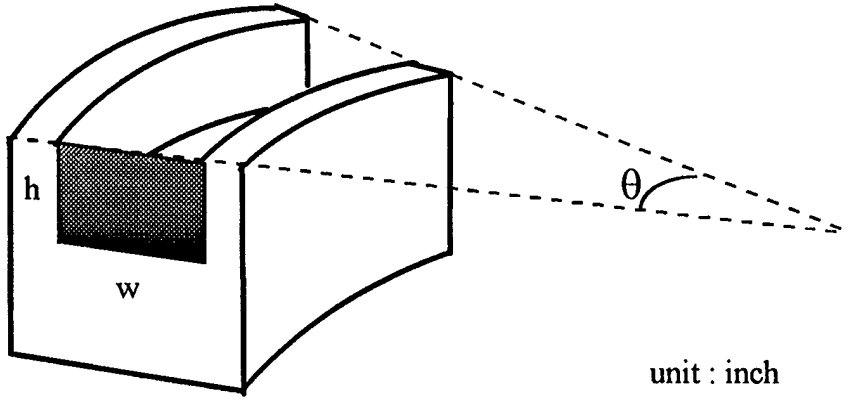

unit : inch

area ratio
= S1/S2
=

θ	#	area ratio	w	h	θ	#	area ratio	w	h
22.5	1 set (5)	0.7	1.694	1.694	5.625	2 set (12)	0.7	1.694	1.694
		0.5	1.432	1.432			0.5	1.432	1.432
		0.3	1.109	1.109			0.3	1.109	1.109
		0.2	0.906	0.906			0.2	0.906	0.906
		0.1	0.640	0.640			0.1	0.640	0.640
11.25	3 set (15)	0.7	1.694	1.694			0	0	0
		0.5	1.432	1.432	total : 32 pieces				
		0.3	1.109	1.109					
		0.2	0.906	0.906					
		0.1	0.640	0.640					

Figure 3-7a. Nominal geometry of the constrictions

unit: cm

θ	S1(cm^2)	S2(cm^2)	area ratio(S1/S2)
22.53 ± 0.06	2.5911	26.447	0.0980
	5.2441		0.1983
	7.8400		0.2964
	13.1769		0.4982
	18.0170		0.6812
11.30 ± 0.05	2.5911	26.447	0.0980
	5.2441		0.1983
	7.8400		0.2964
	13.1769		0.4982
	18.0170		0.6812
5.65 ± 0.02	2.5911	26.447	0.0980
	5.2441		0.1983
	7.8400		0.2964
	13.1769		0.4982
	18.0170		0.6812

Figure 3-7b. Measured geometry of the constrictions.

4. Electronic Instrumentation

Figure 3-8 is a block diagram of the electronic instrumentation used during the measurements. A Hewlett Packard 3562A Dynamic signal analyzer is used to determine the frequency response in the band from 300 Hz to 500 Hz. The signal from this analyzer is amplified by a Techron 5507 power supply amplifier and used as the input signal to the driver. The pole-zero analysis function built into the signal analyzer is used to extract the resonance frequencies from the measured frequency response. Once the resonance frequency is found, a Hewlett Packard 33120A Function/Arbitrary Waveform Generator is used to generate a 1 Vpp sinusoidal signal at the obtained resonance frequency. The signal is also amplified by the same Techron amplifier and used as the input signal to the driver. Either the signal from the analyzer or the function generator signal is monitored on a Tektronics 2336

Oscilloscope. The outputs from the microphones are monitored on the same oscilloscope. A custom made microphone switch board selects each microphone to measure the pressure amplitude at different positions. The microphone output amplitude is measured using a Standford Research 530 Lock In amplifier. In order to measure the temperature of the resonator, an Omega 450 AET thermocouple thermometer type E is used. The thermocouple was calibrated to $\pm 0.1°C$ using a distilled water ice bath. The thermocouple is positioned on the surface of the outer aluminum ring of resonator. The temperature inside resonator is measured frequently and be recorded whenever there is variation.

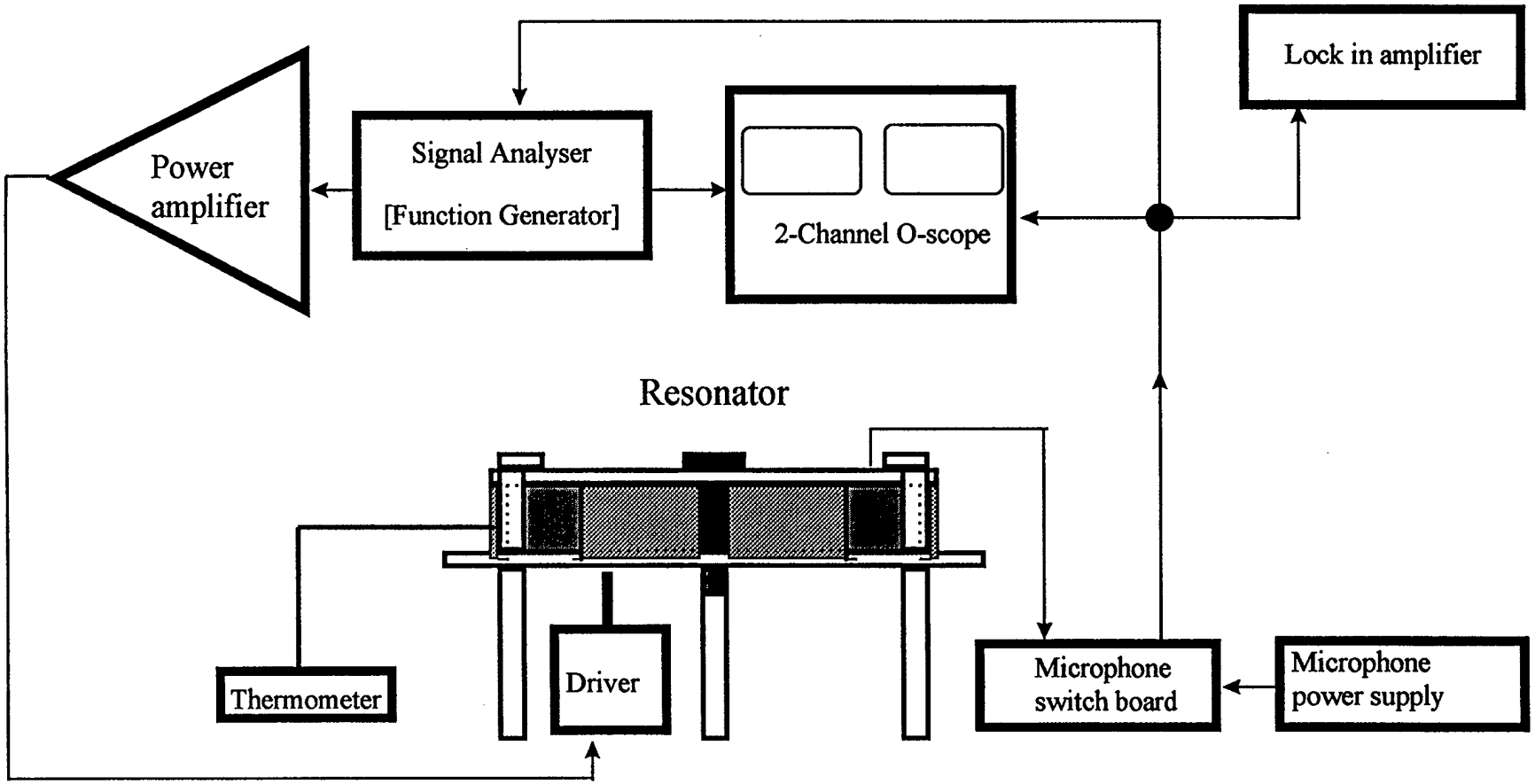

Figure 3-8. Block diagram of instrumentation setup.

C. EXPERIMENTAL PROCEDURE

1. Resonator Setup

Prior to any data acquisition, the resonator is assembled with the constriction in the desired position relative to the driver. For the experiment, three major positions are used. They are 45°, 90° and 180° from driver. The position is measured from the driver to the center of constriction. The top cap is oriented so that 0° is set at the left edge of constriction. The 0° setting is performed by rotation of the cap by hand. For the error measurement of 0° setting, three people conducted rotation of the cap. Each person tried three times and we found that the error by rotation was less than ±0.5°. So, with the mechanical error ±0.25° in drilling the microphone hole, the total error of microphone positioning is less than ±0.75°. With the constriction positioned, the proper amount of vacuum grease is put on the open surface of resonator and the top cap is secured with the clamp bars.

2. Determining Resonator Characteristics

The Hewlett Packard 3562A Dynamic Signal Analyzer is used to characterize the resonator. The swept sine mode of the analyzer provides a sine wave signal to the system at a given range of frequencies. The frequency response of the system is used to determine the resonance frequency and quality factor of several modes of the resonator. When only one mode is excited, the peak pressure amplitude frequency is same as the resonance frequency given by pole-zero analysis. When two modes are excited, pole-zero analysis is used to determine the resonance frequency. The signal analyzer gives poles in the form $a + jb$. The resonance frequency is simply the value of b. The quality factor can be also obtained by $\frac{b}{2a}$ from that form. This method has been explained in the theory chapter. These measurements are performed for each constriction type and each relative position of constriction and driver.

3. Data Collection

Data collection is performed in sets of the positions and different sizes of constriction. Before data collection, the initial ambient temperature and noise level is checked. The output of the Hewlett Packard 6237B Triple output power supply is also set to DC 9V. The measurement is then commenced by getting the resonance frequency from the Hewlett Packard 3562A Dynamic signal analyzer. The microphone switch board is set to the microphone which is closest to the driver. Then the resonance frequency and the temperature of resonator was measured. The procedure to acquire resonance frequency has been mentioned in subsection 2 in this section. Getting quality factor also follows the same procedure previously mentioned. After finding resonance frequency, a data run is commenced by hooking up the Hewlett Packard 33120A function generator to the input amplifier for driver and setting the frequency and voltage. The driving frequency should be the resonance frequency obtained by previous procedure and the voltage is 1 Vpp. The acoustic amplitude is measured with each microphone. With the driver still running, the switch board selects a particular microphone and the value of amplitude at each position is measured with the SR 530 Lock - In amplifier. At this time, if there is variation in the resonator temperature, it is noted. All data recorded from the 16 microphones are scaled by the correction factor obtained from microphone calibration. The corrected data go to computer program to plot mode shape. This concludes data acquisition of one mode.

Procedure for Wave Guide Characterization Collection

1. Date : / /97 (~)

2. Ambient Condition
   Room Temper : °C (K) / Speed of Sound = m/s
   Ambient Pressure: mbar / Initial Temp of resonator: °C

3. Configuration (Constriction)
   # of Const. : EA / Size : °
   Area Ratio :
   Position of Const. : ° (CCW / CW) from driver
   Position of Driver : °

4. Resonance Freq: / Q: / Mode:

5. Source information
   Input : Vpp / Type of source :

6. Data : WG with Const(s) ⇒ T (mode)

Receiver	Vrms of receiver	Corerected Data	Temp of Torus	Resonance Freq	Q
1 (000)		( )			
2 (006)		( )			
3 (012)		( )			
4 (018)		( )			
5 (024)		( )			
6 (030)		( )			
7 (060)		( )			
8 (090)		( )			
9 (120)		( )			
10 (150)		( )			
11 (180)		( )			
12 (210)		( )			
13 (240)		( )			
14 (270)		( )			
15 (300)		( )			
16 (330)		( )			

Figure 3-9. Data collection form.

IV. RESULTS AND DISCUSSION

The purpose of this chapter is to show the comparison between theory and experimental results. The result of resonance frequency measurements are discussed first and then the mode shapes.

A. RESONANCE FREQUENCIES

The measured resonance frequencies are determined from pole-zero analysis of the frequency response. Because the resonance frequencies were measured at different temperatures, they were corrected to 20°C in order to make comparison of data recorded at various temperatures with the theoretical resonance frequencies more straightforward. The equation for conversion is

$$f_{20} = f_{measured}\sqrt{\frac{1+\frac{20}{273}}{1+\frac{T_{measured}}{273}}}. \qquad (4.1)$$

The theoretical resonance frequencies were calculated for two different cases. One case was without end corrections and the other was with end corrections. All the results are listed in Tables 4-1 and 4-2. Tables 4-1a and 4.2a list the resonance frequencies for the low (L) and high (H) modes for the various constriction lengths and area ratios. Tables 4-1b and 4-2b lists the temperatures at which the frequencies were measured. Tables 4-1c and 4-2c list the 20°C-corrected frequencies. Tables a, b and c are identical for Tables 4-1 and 4-2. Tables 4-1d and 4-2d give the calculated resonance frequencies. Table 4-1d ignores end corrections. Table 4-2d includes end corrections as calculated from higher order non propagating modes. Tables 4-1e and 4-2e list the percent error between measured and calculated resonance frequencies.

It is evident that the inclusion of end corrections has little effect on the prediction for the high modes. In both cases the average error is approximately 0.15%. However, end corrections are very important for the low mode. This point is evident from Fig. 4-1 where it is seen that inclusion of end corrections is important for the low mode only.

Figure. 4-1 shows the 20°C-corrected resonance frequencies as well the predicted results (without and with end corrections) as functions of area ratio.

In this section it was shown that end corrections are an important factor to include when calculating resonance frequencies, especially for the low mode. In the next section, it is shown that they are also important when calculating mode shapes.

1. Comparison of Measured Resonance Frequency with Calculated Results without End Corrections

AR	0.1		0.2		0.3		0.5		0.7		1.0
size	L	H	L	H	L	H	L	H	L	H	
L/16	308.2	461.5	347.8	458.1	373.5	455.4	405.4	449.3	421.9	444.0	435.6
L/32	328.7	449.6	368.7	447.8	391.7	446.4	416.5	443.6	426.9	439.3	
L/64	348.6	443.1	384.2	441.4	402.6	440.7	422.1	439.3	431.1	438.6	

Table 4-1a. Measured resonance frequencies for different constrictions.

AR	0.1		0.2		0.3		0.5		0.7		1.0
size	L	H	L	H	L	H	L	H	L	H	
L/16	22.5	22.5	21.4	21.4	21.8	21.8	22.0	22.0	22.4	22.4	22.1
L/32	23.9	23.9	23.3	23.3	23.6	23.6	23.7	23.7	21.6	21.6	
L/64	24.0	24.0	22.3	22.3	22.3	22.3	22.3	22.3	23.5	23.5	

Table 4-1b. Temperatures for each measurement from table 4-1a.

AR	0.1		0.2		0.3		0.5		0.7		1.0
size	L	H	L	H	L	H	L	H	L	H	
L/16	306.9	459.5	347.0	457.0	372.4	454.0	404.0	447.8	420.2	442.2	434.0
L/32	326.5	446.6	366.6	445.3	389.3	443.7	413.9	440.8	425.7	438.1	
L/64	346.2	440.1	382.7	439.7	401.0	439.0	420.5	437.6	428.5	436.0	

Table 4-1c. Measured resonance frequencies corrected to 20°C.

AR	0.1		0.2		0.3		0.5		0.7		1.0
size	L	H	L	H	L	H	L	H	L	H	
L/16	317.6	459.2	359.7	456.1	383.2	453.1	409.2	447.2	421.5	442.0	434.2
L/32	349.3	445.9	387.3	444.5	404.2	443.1	420.2	440.2	427.1	437.7	
L/64	381.1	439.5	407.7	438.8	417.8	438.1	426.5	436.7	430.1	435.5	

Table 4-1d. Calculated resonance frequencies at 20°C, without end corrections.

AR	0.1		0.2		0.3		0.5		0.7		1.0
size	L	H	L	H	L	H	L	H	L	H	
L/16	3.48	0.07	3.71	0.18	2.91	0.21	1.29	0.13	0.32	0.04	0.05
L/32	6.98	0.16	5.65	0.19	3.83	0.14	1.53	0.13	0.33	0.10	
L/64	10.1	0.13	6.54	0.20	4.19	0.20	1.44	0.20	0.38	0.11	

Table 4-1e. Percent error between measured and calculated resonance frequency.

2. Comparison of Measured Resonance Frequency with Calculated Results with End Corrections

AR	0.1		0.2		0.3		0.5		0.7		1.0
size	L	H	L	H	L	H	L	H	L	H	
L/16	308.2	461.5	347.8	458.1	373.5	455.4	405.4	449.3	421.9	444.0	435.6
L/32	328.7	449.6	368.7	447.8	391.7	446.4	416.5	443.6	426.9	439.3	
L/64	348.6	443.1	384.2	441.4	402.6	440.7	422.1	439.3	431.1	438.6	

Table 4-2a. Measured resonance frequencies for different constrictions.

AR	0.1		0.2		0.3		0.5		0.7		1.0
size	L	H	L	H	L	H	L	H	L	H	
L/16	22.5	22.5	21.4	21.4	21.8	21.8	22.0	22.0	22.4	22.4	22.1
L/32	23.9	23.9	23.3	23.3	23.6	23.6	23.7	23.7	21.6	21.6	
L/64	24.0	24.0	22.3	22.3	22.3	22.3	22.3	22.3	23.5	23.5	

Table 4-2b. Temperatures for each measurement from table 4-2a.

AR	0.1		0.2		0.3		0.5		0.7		1.0
size	L	H	L	H	L	H	L	H	L	H	
L/16	306.9	459.5	347.0	457.0	372.4	454.0	404.0	447.8	420.2	442.2	434.0
L/32	326.5	446.6	366.6	445.3	389.3	443.7	413.9	440.8	425.7	438.1	
L/64	346.2	440.1	382.7	439.7	401.0	439.0	420.5	437.6	428.5	436.0	

Table 4-2c. Measured resonance frequencies corrected to 20°C.

AR	0.1		0.2		0.3		0.5		0.7		1.0
size	L	H	L	H	L	H	L	H	L	H	
L/16	305.9	459.1	346.0	456.0	371.7	453.0	403.8	447.1	419.5	442.0	434.2
L/32	326.2	445.9	366.2	444.4	388.7	443.0	414.1	440.2	424.9	437.7	
L/64	345.6	439.5	381.4	438.8	400.0	438.1	420.0	436.8	427.8	435.5	

Table 4-2d. Calculated resonance frequencies at 20°C with end corrections.

AR	0.1		0.2		0.3		0.5		0.7		1.0
size	L	H	L	H	L	H	L	H	L	H	
L/16	0.34	0.08	0.28	0.21	0.20	0.21	0.04	0.15	0.16	0.05	0.05
L/32	0.10	0.16	0.11	0.19	0.15	0.15	0.04	0.14	0.18	0.09	
L/64	0.17	0.13	0.34	0.20	0.24	0.20	0.12	0.19	0.15	0.12	

Table 4-2e. Percent error between measured and calculated resonance frequency.

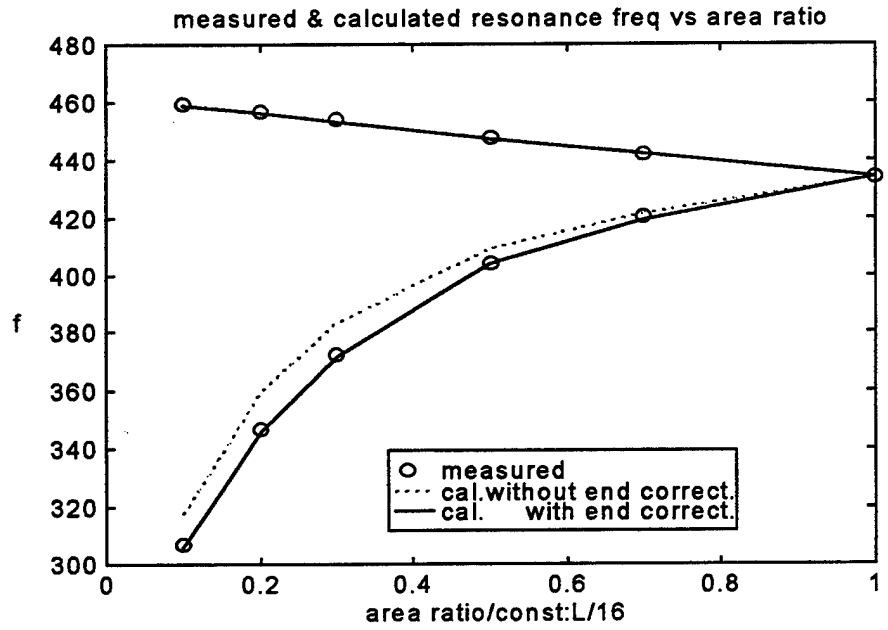

Figure 4-1a. Comparison of calculated and measured resonance frequencies versus area ratio for the L/16 constriction.

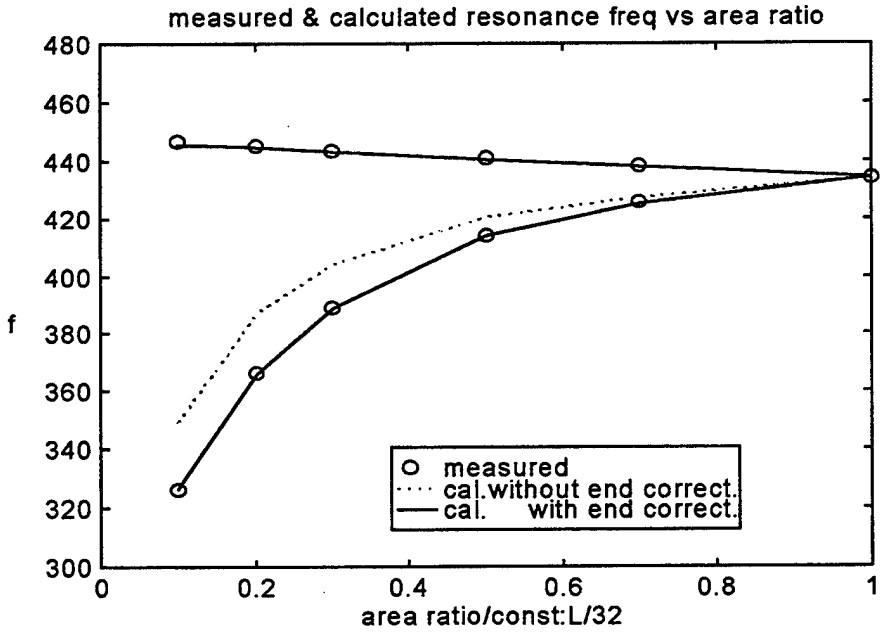

Figure 4-1b. Comparison of calculated and measured resonance frequencies versus area ratio for the L/32 constriction.

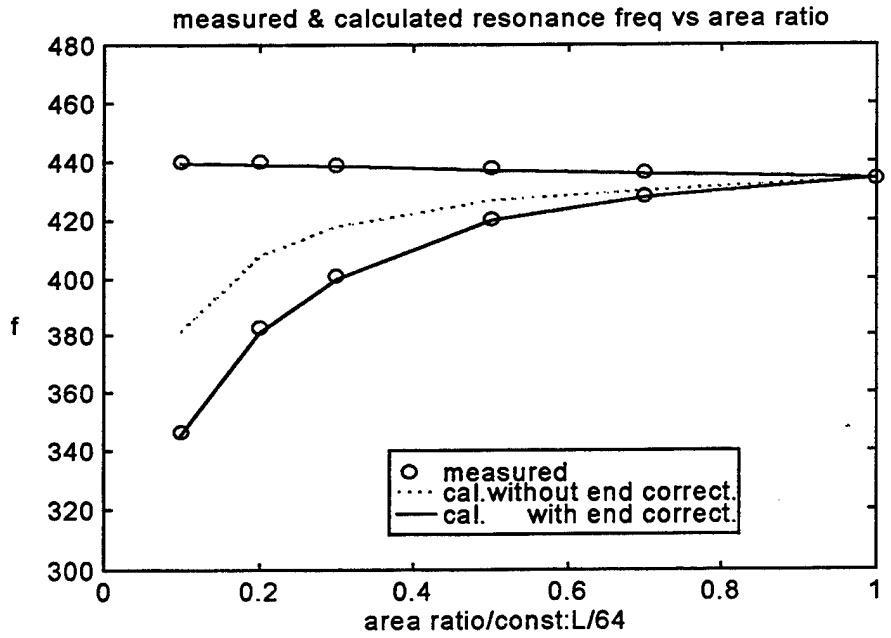

Figure 4-1c. Comparison of calculated and measured resonance frequencies versus area ratio for the L/64 constriction.

B. MODE SHAPES

Figures 4-2a and b show the comparison of the measured and computed mode shapes for the L/16, 0.1 area ratio constriction. The measurements have been normalized to the highest value of pressure amplitude. The amplitude of the mode shape is determined from least squares fit to the measured data. The driver is located 45° from the constriction. Figure 4-2a shows the results for the high mode. It is seen that there is good agreement between the measured and predicted mode shapes, even though end corrections are not included in the calculation. The driver is located at a place where both modes should be excited. However, the modes are well separated with this constriction, so there is little excitation of the low mode. Single mode excitation is indicated by a high standing wave ratio from the mode shape.

Figure 4-2b shows the mode shape for the low mode. The agreement between the measured and calculated mode shape is significantly worse than with the high mode.

Figures 4-2c and d show the mode shapes again but this time end corrections are taken into account. Comparing Fig. 4-2c and 4-2a, it is seen that end corrections have little effect on the high mode. However, they are very important for the low mode, just as was discussed in the previous section. Figure 4-2d shows that when end corrections are taken into account, the agreement between calculated and measured mode shape improves significantly.

Figures 4-3a and b show the mode shapes for the case when the driver is located 45° from the L/32, 0.7 area ratio constriction. In the case the constriction is relatively short and the area ratio is relatively large. As a result, the modes are not well separated. So although the driver is excited at the resonance frequency of one mode, there is significant excitation of the other mode, as evidenced by the low standing wave ratio.

Figure 4-3a shows the mode shape when the resonator is driven at the high mode resonance frequency. End correction are ignored in the calculation. The agreement between measured and calculated mode shape is not as good as in the previous, well separated-mode case (Fig. 4-2). Figure 4-3b shows the results for the low mode. Here the agreement between theory and experiment is worse. In both cases, the standing wave ratio is noticeably lower that in the well-separated case.

Figure 4-3c and d show the effect of including end corrections. There is some improvement in the agreement for the high mode case. There is considerable improvement in the agreement for the low mode, and some improvement for the high mode. Many other comparisons are provided in the Appendix. The cases presented in this chapter are representative. The overall agreement in mode shape is good even in the overlapping-mode case.

The results of this chapter indicate that end corrections are important both for calculation of resonance frequency and mode shapes. Also end corrections are more important for the low mode. This is because the acoustic impedance of the low mode is low in comparison to that of the high mode. The addition of the effective impedance of the end corrections is of more consequence, then, to the low mode.

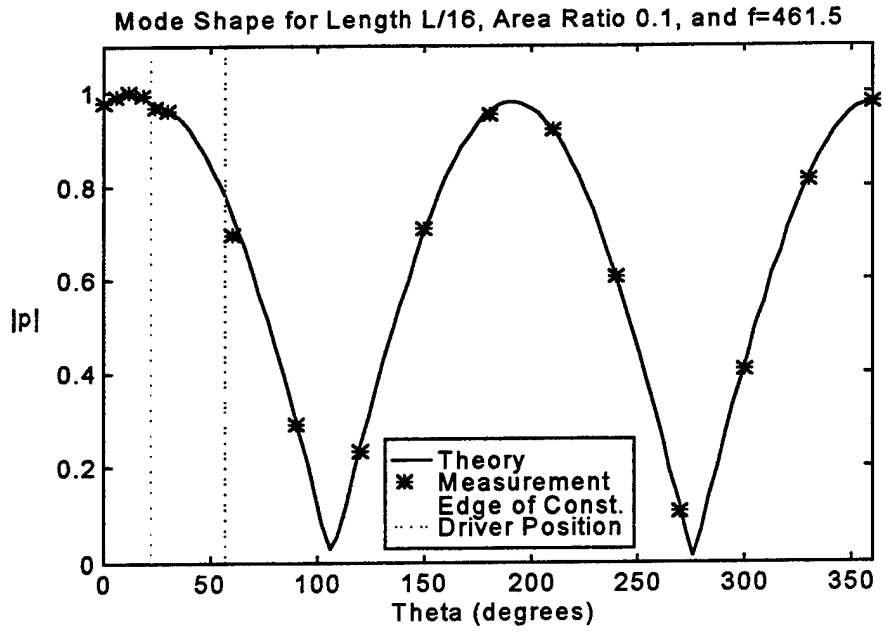

Figure 4-2a. Mode shape for the high mode when the driver is located 45° from the constriction having length of L/16 and area ratio of 0.1. End corrections are not included in the calculation.

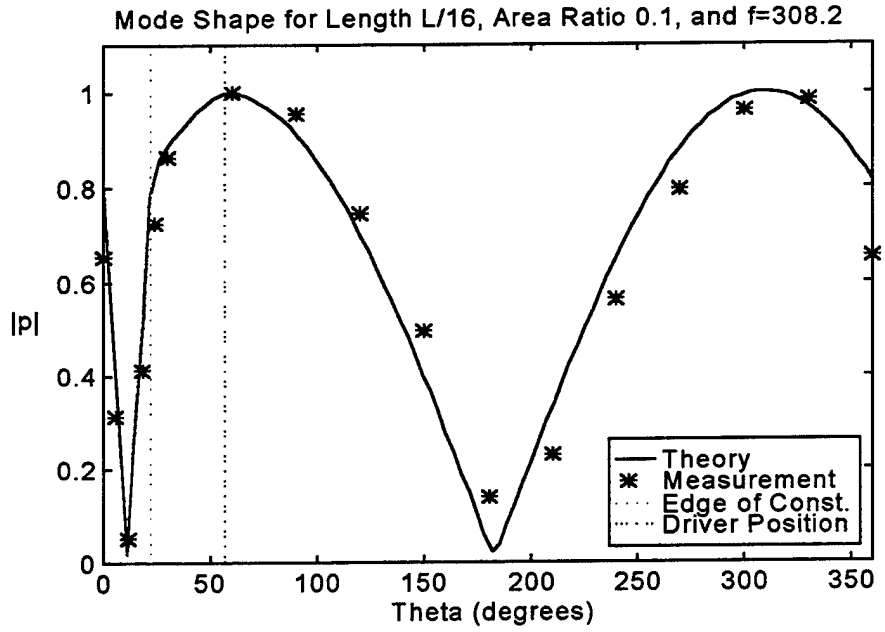

Figure 4-2b. Mode shape for the low mode when the driver is located 45° from the constriction having length of L/16 and area ratio of 0.1. End corrections are not included in the calculation.

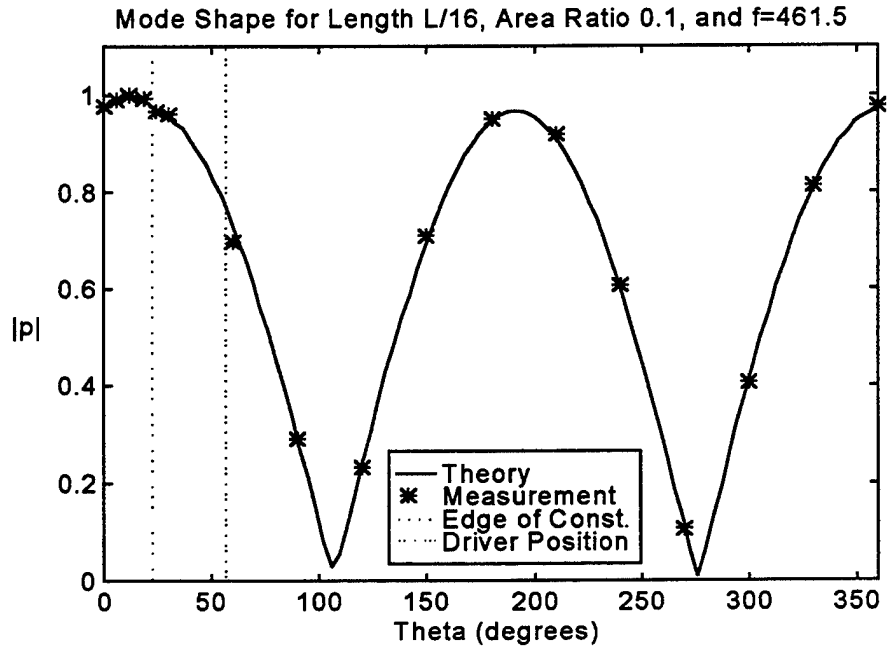

Figure 4-2c. Mode shape for the high mode when the driver is located 45° from the constriction having length of L/16 and area ratio of 0.1. End corrections are included in the calculation.

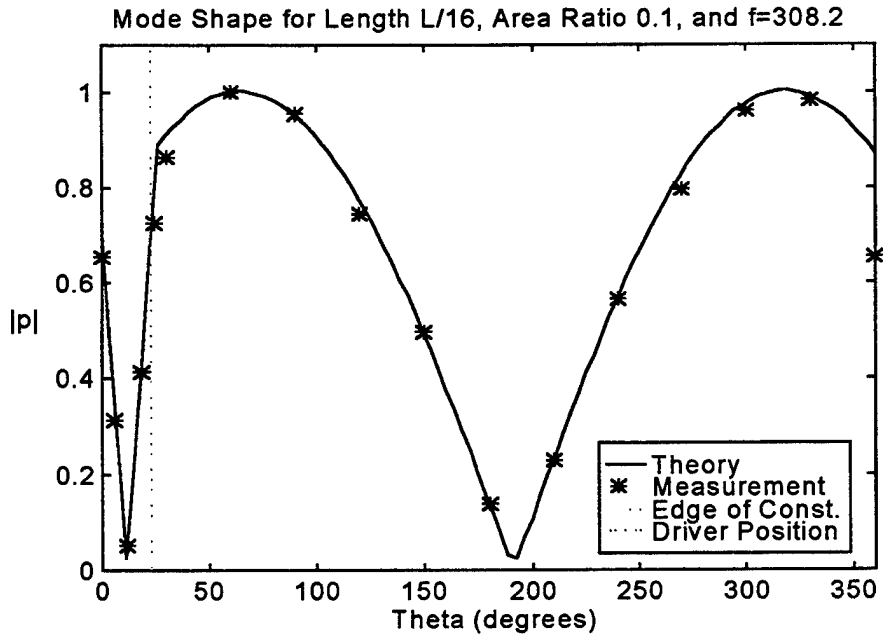

Figure 4-2d. Mode shape for the low mode when the driver is located 45° from the constriction having length of L/16 and area ratio of 0.1. End corrections are included.

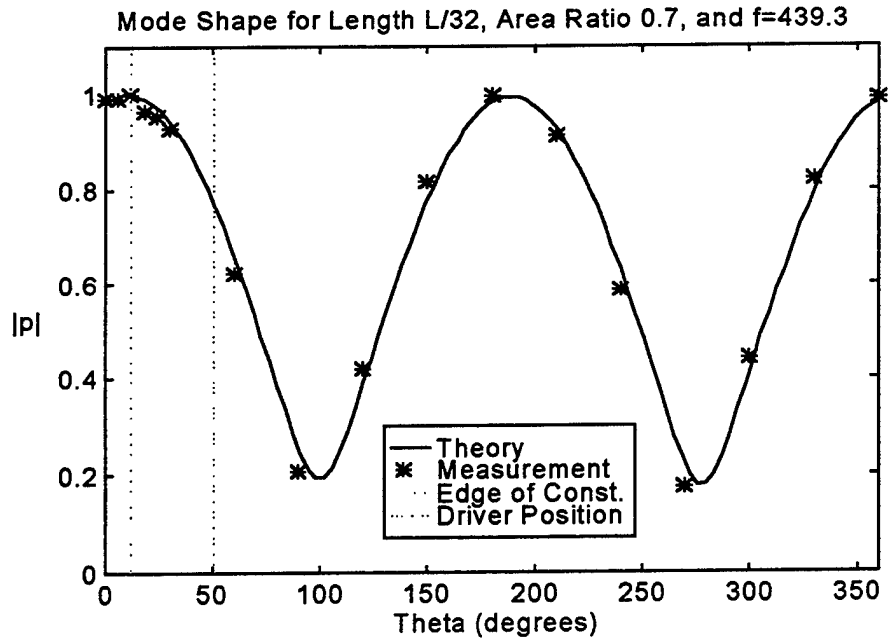

Figure 4-3a. Mode shape for the high mode when the driver is located 45° from the constriction having length of L/32 and area ratio of 0.7. End corrections are not included.

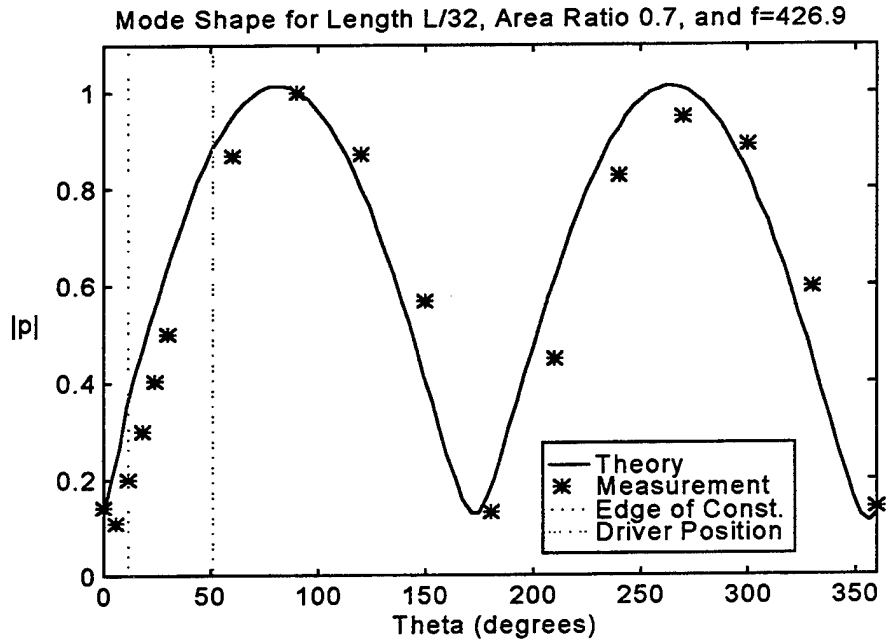

Figure 4-3b. Mode shape for the low mode when the driver is located 45° from the constriction having length of L/32 and area ratio of 0.7. End corrections are not included.

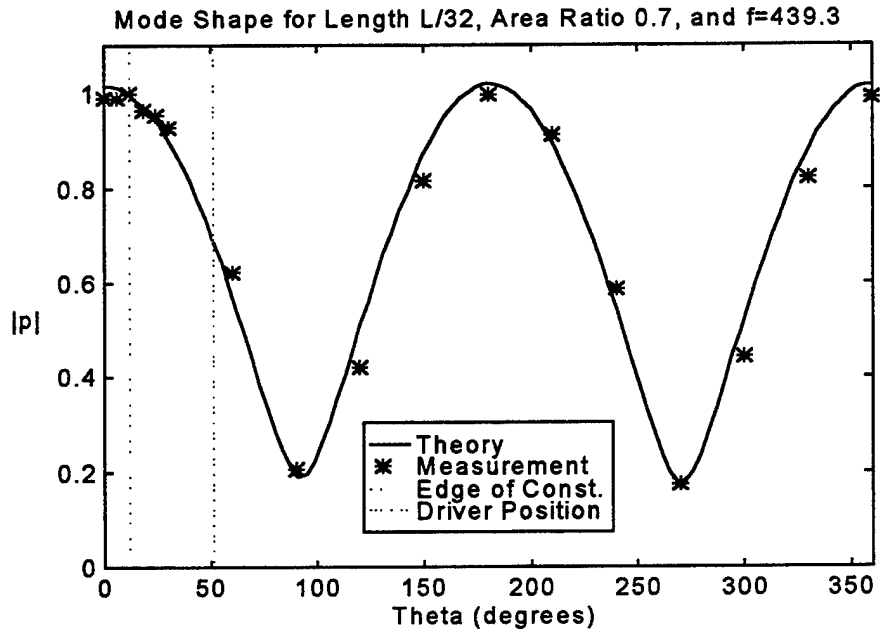

Figure 4-3c. Mode shape for the high mode when the driver is located 45° from the constriction having length of L/32 and area ratio of 0.7. End corrections are included

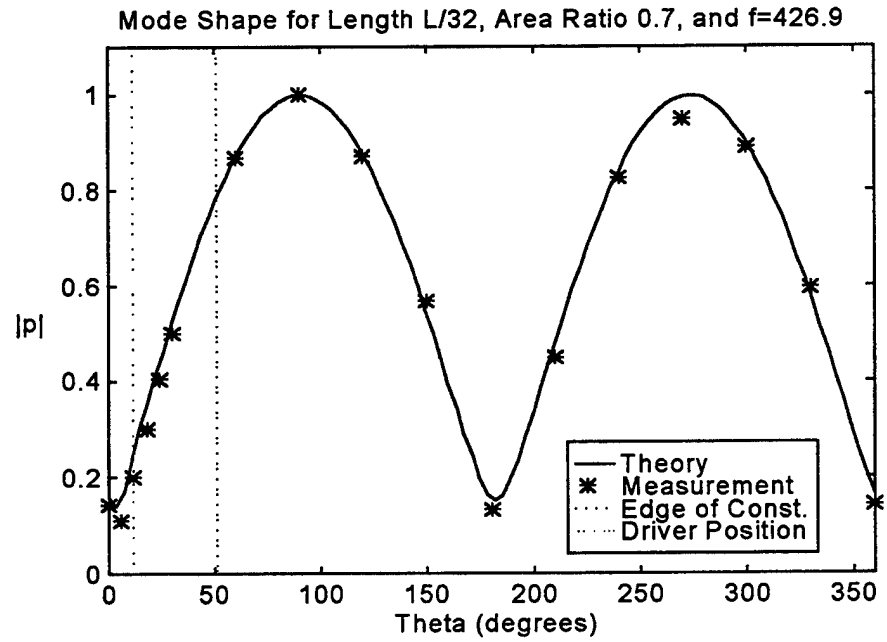

Figure 4-3d. Mode shape for the low mode when the driver is located 45° from the constriction having length of L/32 and area ratio of 0.7. End corrections are included

V. SUMMARY AND CONCLUSIONS

The purpose of this thesis is to investigate frequency splitting and mode shapes in a constricted annular resonator. The measurements are intended to serve as preliminary verification of a model predicting the performance of an annular thermoacoustic prime mover.

The constriction splits the degeneracy of the plane wave-like modes of a uniform cross section annular resonator. One mode has a pressure antinode at the constriction, the other a pressure node. The resonance frequency of the former is higher than that of the latter. The difference in resonance frequency depends upon the length and porosity of the constriction. The effects of dissipation cause the frequency responses of the individual modes to overlap.

An equivalent plane wave model is developed to predict the resonance frequencies and mode shapes. The experimental resonance frequencies are determined from pole-zero analysis of the measured frequency response.

It is shown that it is critical to take into account end corrections at the constriction to get good agreement between the measured and predicted results. End corrections are more important for the low mode than the high mode.

In general the percent error between measured and predicted resonance frequencies is less than 0.2 % for high mode and 0.3 % for the low mode. The measured mode shape are also in good agreement with predictions.

The results of this thesis indicate that the simple constricted annular resonator is well understood. The sensitivity of the resonance frequencies and mode shapes to end corrections indicates that the annular resonator is a good geometry for investigating these effects further. For instance, how does one model the end corrections for a thermoacoustic stack? Are the end corrections for a stack and a constriction having the same porosity substantially different? These questions are left for future work.

APPENDIX DATA TABLE & MODE SHAPE

Experiment 1.

Constriction	length: L/ 16 , area ratio: 0.1 , angle from driver:180°				
Resonance. frq.: 463.7 Hz		Q:109	Mode: high		Temp: 24.6°C
Microphone # (θ)	Vrms (mV)	Corrected Data	Microphone # (θ)	Vrms (mV)	Corrected Data
1 (000)	70.5	70.5	9 (120)	13.1	16.6
2 (006)	67.3	69.7	10 (150)	33.6	50.1
3 (012)	55.9	71.5	11 (180)	79.4	67.0
4 (018)	52.8	70.5	12 (210)	45.4	65.1
5 (024)	44.3	69.4	13 (240)	33.1	43.0
6 (030)	58.9	69.1	14 (270)	5.8	7.7
7 (060)	39.2	53.1	15 (300)	27.4	28.3
8 (090)	15.9	20.8	16 (330)	48.6	57.0

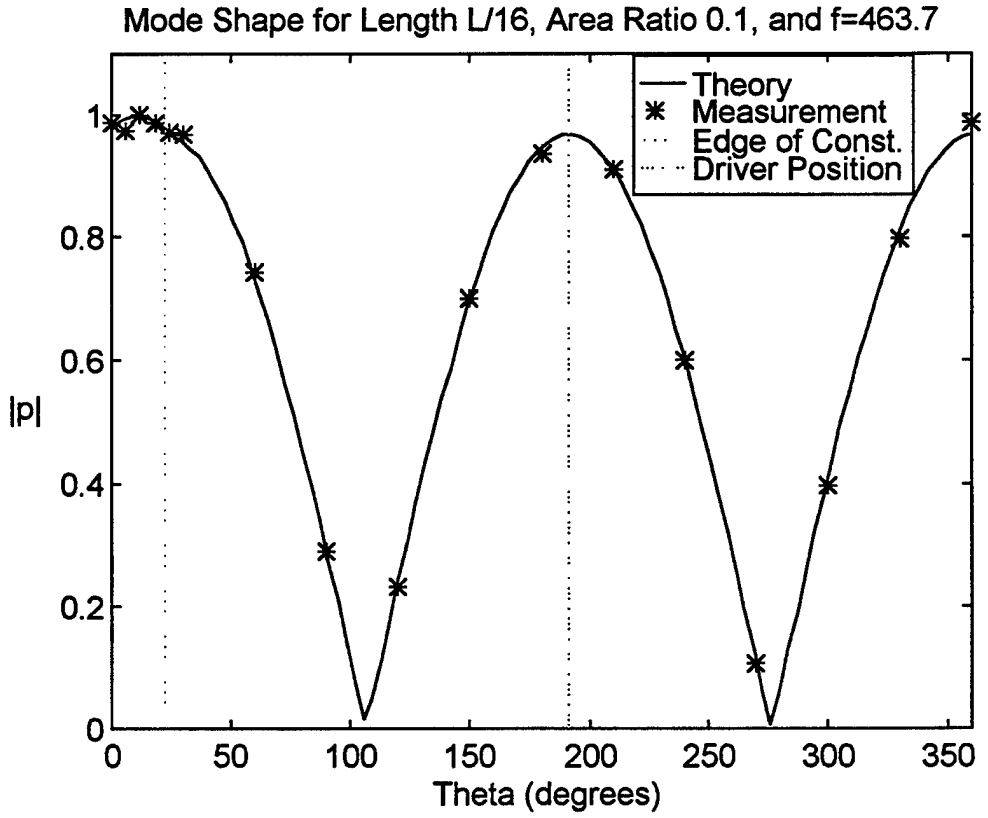

Experiment 2.

Constriction	length: L/ 16 , area ratio: 0.1 , angle from driver:90°				
Resonance. frq.: 308.8 Hz		Q: 68.5	Mode: low		Temp: 24.5°C
Microphone # (θ)	Vrms (mV)	Corrected Data	Microphone # (θ)	Vrms (mV)	Corrected Data
1 (000)	39.5	39.5	9 (120)	35.6	44.7
2 (006)	17.2	17.6	10 (150)	19.8	29.5
3 (012)	3.4	4.3	11 (180)	9.5	8.1
4 (018)	20.0	26.0	12 (210)	9.7	13.8
5 (024)	28.6	44.8	13 (240)	26.2	34.1
6 (030)	45.4	53.0	14 (270)	35.6	47.9
7 (060)	44.9	60.6	15 (300)	54.9	57.8
8 (090)	43.4	57.3	16 (330)	49.7	58.7

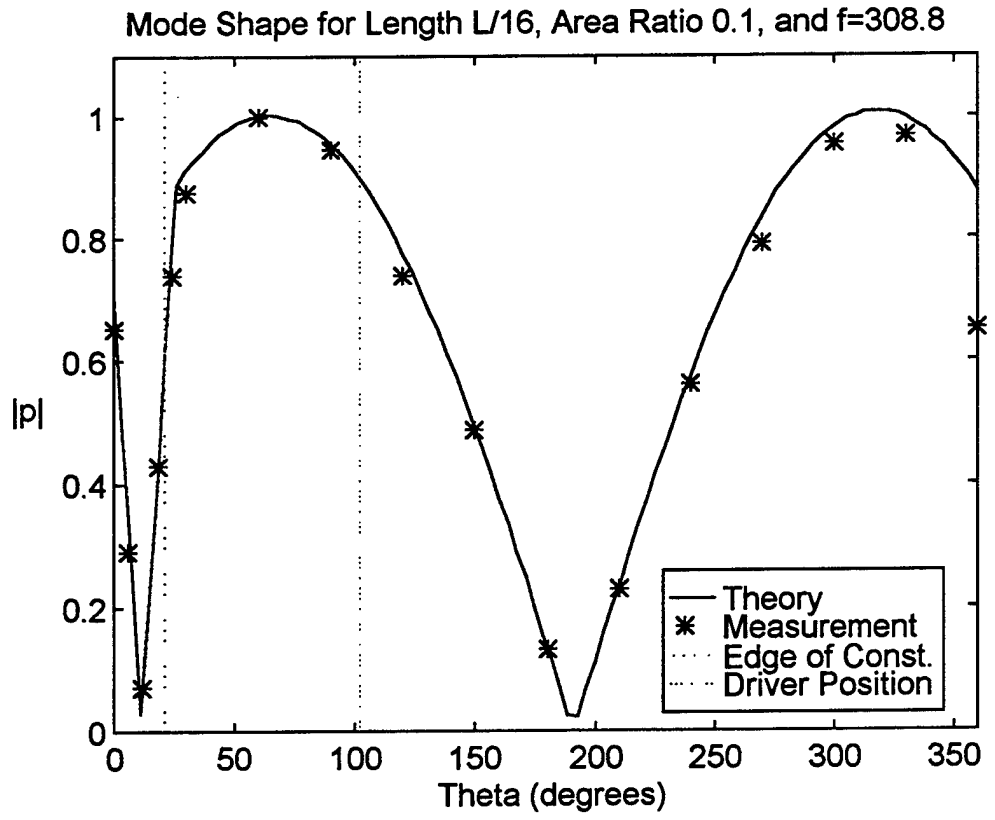

Experiment 3.

Constriction	length: L/ 16 , area ratio: 0.1 , angle from driver:45°				
Resonance frq.: 461.5 Hz		Q: 98	Mode: high		Temp: 22.5°C
Microphone # (θ)	Vrms (mV)	Corrected Data	Microphone # (θ)	Vrms (mV)	Corrected Data
1 (000)	49.8	49.8	9 (120)	9.4	11.9
2 (006)	48.7	50.4	10 (150)	24.2	36.1
3 (012)	39.8	50.9	11 (180)	57.4	48.5
4 (018)	37.8	50.5	12 (210)	32.6	46.8
5 (024)	31.4	49.2	13 (240)	23.7	30.8
6 (030)	41.7	48.9	14 (270)	4.1	5.5
7 (060)	27.8	35.5	15 (300)	20.0	20.7
8 (090)	11.3	14.8	16 (330)	35.3	41.4

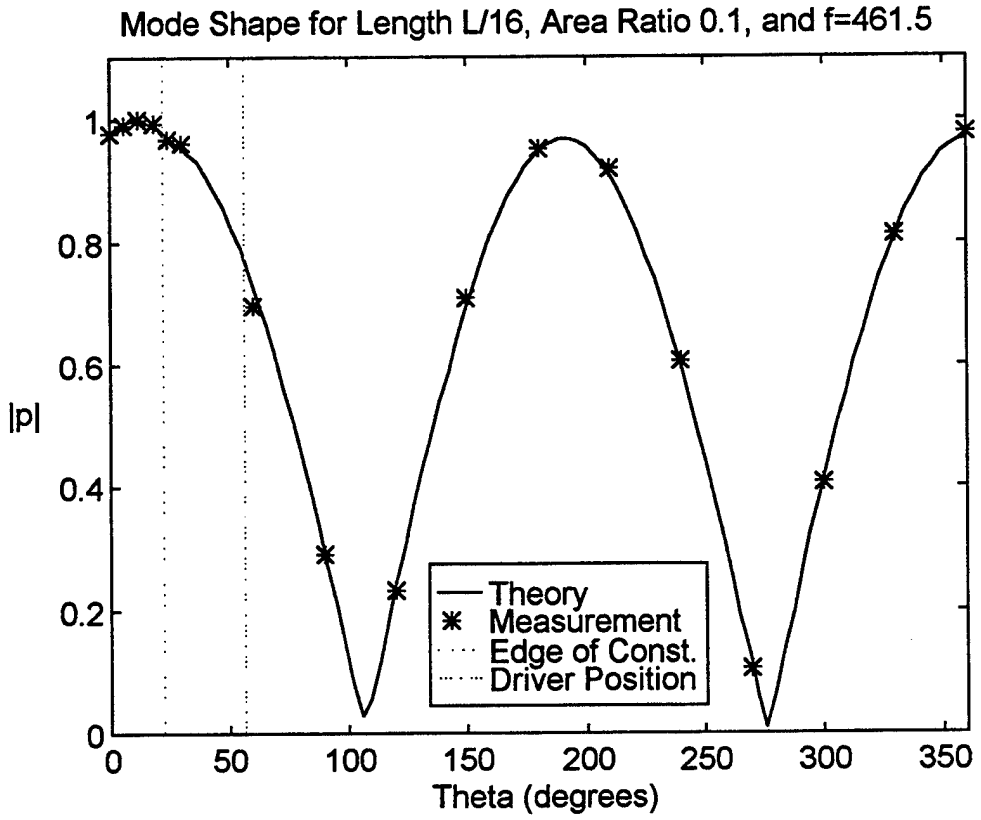

Experiment 4.

Constriction	length: L/ 16 , area ratio: 0.1 , angle from driver:45°				
Resonance frq.: 308.2 Hz		Q: 58	Mode: low		Temp: 22.5°C
Microphone # (θ)	Vrms (mV)	Corrected Data	Microphone # (θ)	Vrms (mV)	Corrected Data
1 (000)	36.4	36.4	9 (120)	33.0	41.5
2 (006)	17.0	17.4	10 (150)	18.6	27.7
3 (012)	2.3	2.9	11 (180)	9.2	7.8
4 (018)	17.7	23.0	12 (210)	8.9	12.7
5 (024)	25.8	40.4	13 (240)	24.2	31.5
6 (030)	41.3	48.2	14 (270)	33.0	44.4
7 (060)	41.3	55.7	15 (300)	50.8	53.5
8 (090)	40.3	53.2	16 (330)	46.4	54.8

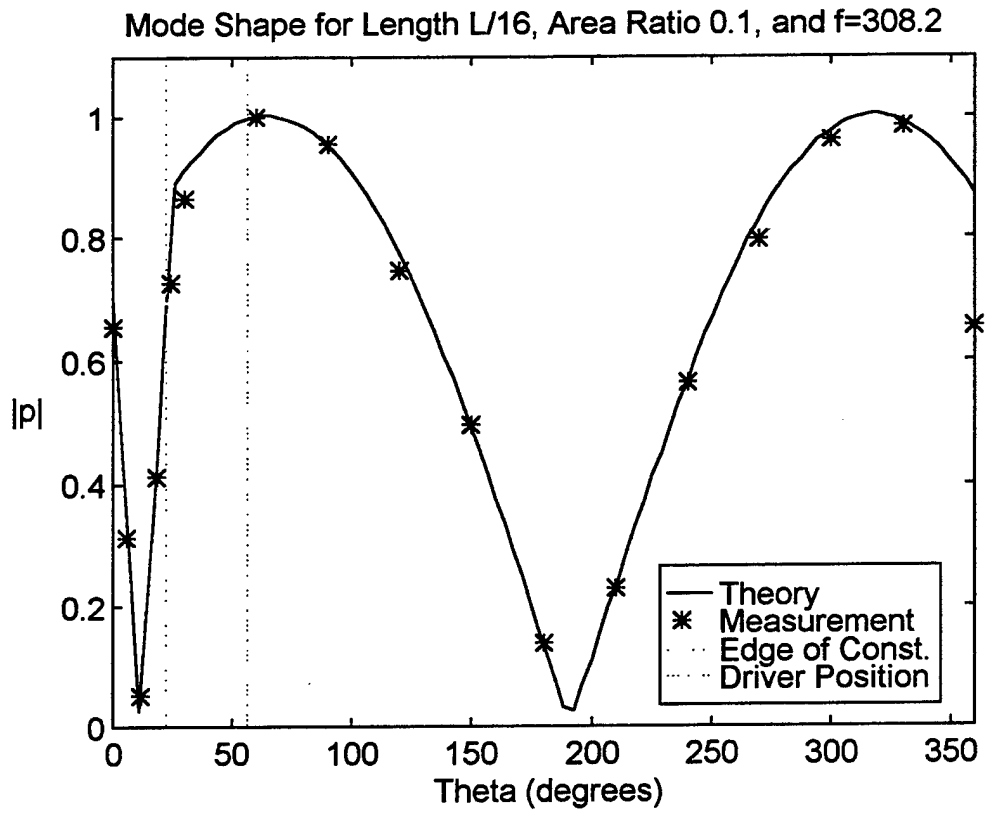

Experiment 5.

Constriction	length: L/ 32 , area ratio: 0.1 , angle from driver:180°				
Resonance frq.: 448.9 Hz		Q: 111	Mode: high		Temp: 22.9°C
Microphone # (θ)	Vrms (mV)	Corrected Data	Microphone # (θ)	Vrms (mV)	Corrected Data
1 (000)	69.6	69.6	9 (120)	20.6	26.0
2 (006)	67.2	69.5	10 (150)	37.9	56.5
3 (012)	55.2	70.5	11 (180)	82.8	69.9
4 (018)	51.7	68.9	12 (210)	44.0	63.1
5 (024)	42.9	67.1	13 (240)	29.7	38.5
6 (030)	56.1	65.7	14 (270)	2.5	3.3
7 (060)	32.9	44.5	15 (300)	30.7	31.7
8 (090)	7.6	9.9	16 (330)	50.2	59.0

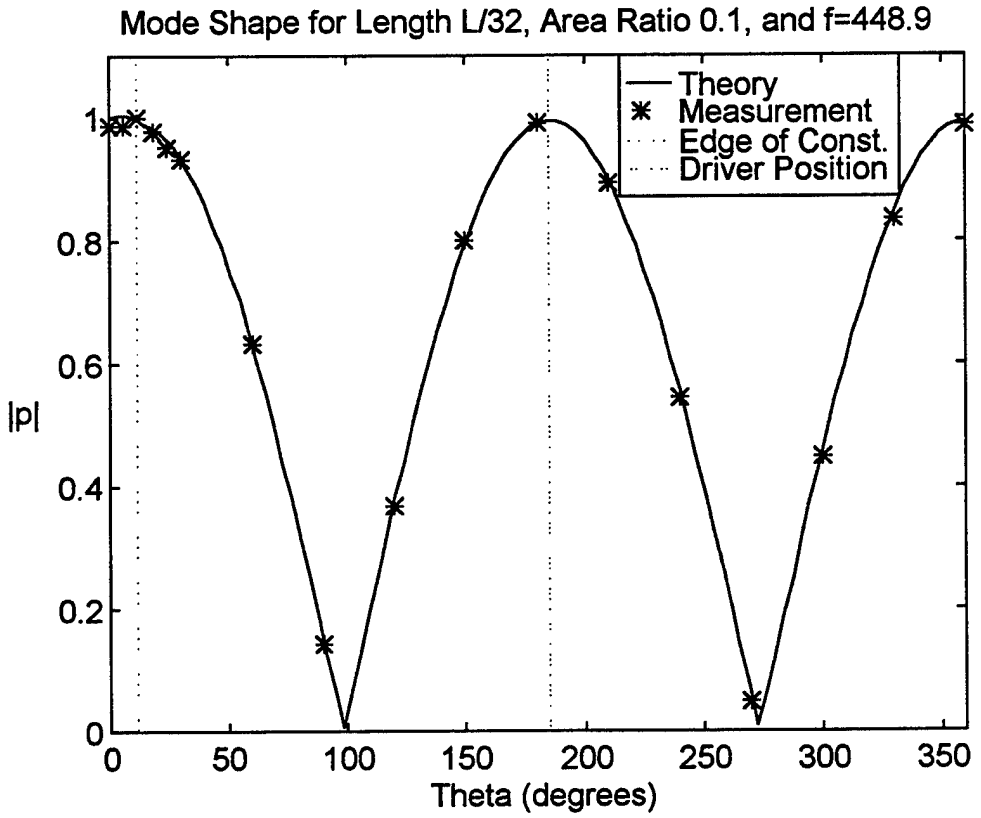

Experiment 6.

Constriction	length: L/ 32 , area ratio: 0.1 , angle from driver:90°				
Resonance frq.: 328.7 Hz		Q: 69.4	Mode: low		Temp: 22.3°C
Microphone # (θ)	Vrms (mV)	Corrected Data	Microphone # (θ)	Vrms (mV)	Corrected Data
1 (000)	20.3	20.3	9 (120)	28.7	35.9
2 (006)	3.8	3.9	10 (150)	15.0	22.2
3 (012)	21.2	26.7	11 (180)	4.0	3.4
4 (018)	27.9	36.4	12 (210)	10.9	15.5
5 (024)	26.1	40.8	13 (240)	24.8	32.2
6 (030)	37.4	43.6	14 (270)	31.6	42.3
7 (060)	36.7	49.7	15 (300)	46.0	48.3
8 (090)	35.6	45.9	16 (330)	38.9	45.8

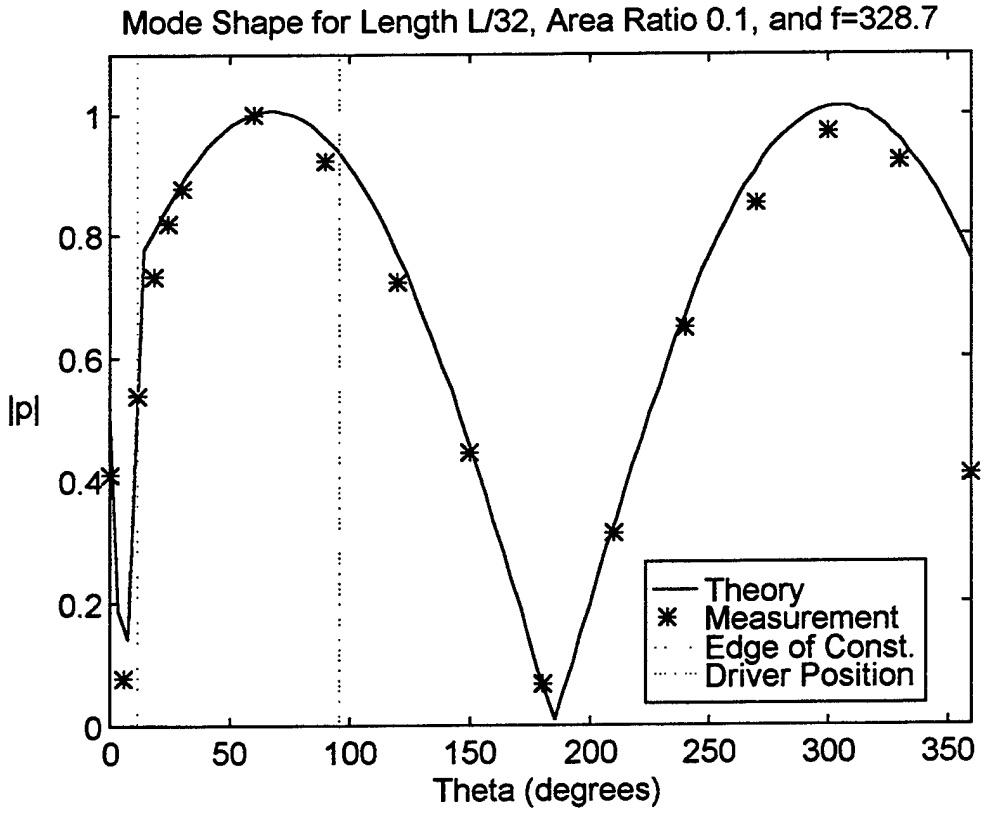

Experiment 7.

Constriction	length: L/ 32 , area ratio: 0.1 , angle from driver:45°				
Resonance frq.: 449.6 Hz		Q: 90.3	Mode: high		Temp: 23.8°C
Microphone # (θ)	Vrms (mV)	Corrected Data	Microphone # (θ)	Vrms (mV)	Corrected Data
1 (000)	44.7	44.7	9 (120)	13.3	16.8
2 (006)	41.7	43.1	10 (150)	24.4	36.4
3 (012)	35.1	44.8	11 (180)	52.5	44.3
4 (018)	33.2	44.3	12 (210)	28.3	40.6
5 (024)	27.4	42.9	13 (240)	19.2	24.9
6 (030)	35.9	42.0	14 (270)	1.7	2.3
7 (060)	21.0	28.4	15 (300)	19.9	20.6
8 (090)	4.9	6.4	16 (330)	32.5	38.2

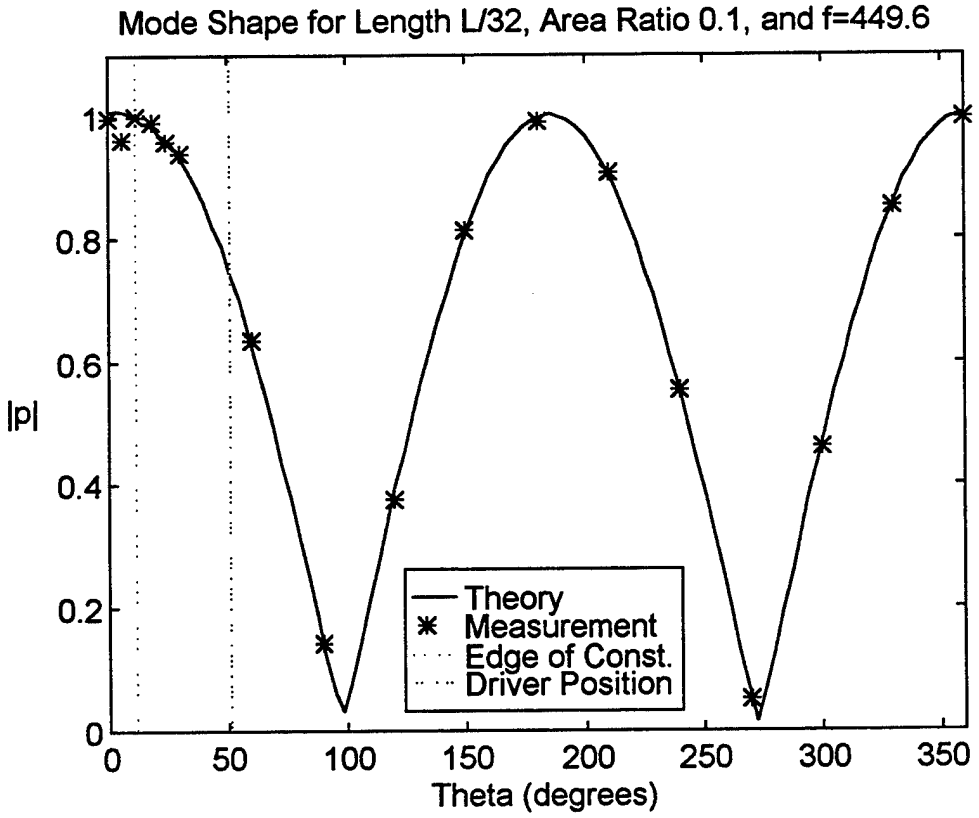

Experiment 8.

Constriction	length: L/ 32 , area ratio: 0.1 , angle from driver:45°				
Resonance frq.: 328.7 Hz		Q: 56	Mode: low		Temp: 23.8°C
Microphone # (θ)	Vrms (mV)	Corrected Data	Microphone # (θ)	Vrms (mV)	Corrected Data
1 (000)	21.6	21.6	9 (120)	29.0	36.3
2 (006)	2.5	2.6	10 (150)	15.3	22.7
3 (012)	20.7	26.0	11 (180)	4.3	3.7
4 (018)	28.1	36.6	12 (210)	11.0	15.7
5 (024)	26.1	40.8	13 (240)	24.9	32.4
6 (030)	37.6	43.9	14 (270)	31.8	42.6
7 (060)	37.0	50.1	15 (300)	46.5	48.8
8 (090)	35.9	46.3	16 (330)	39.5	46.5

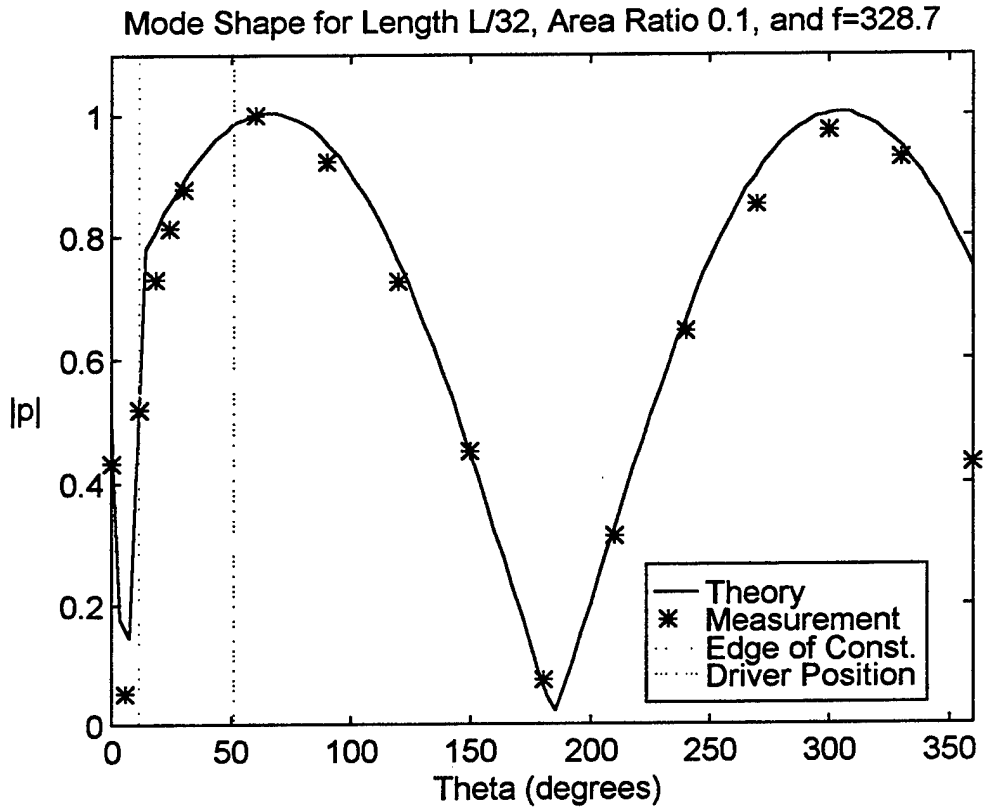

Experiment 9.

Constriction	length: L/ 64 , area ratio: 0.1 , angle from driver:180°				
Resonance frq.: 443.2 Hz		Q: 116	Mode: high		Temp: 22.3°C
Microphone # (θ)	Vrms (mV)	Corrected Data	Microphone # (θ)	Vrms (mV)	Corrected Data
1 (000)	72.8	72.8	9 (120)	24.9	31.4
2 (006)	67.7	69.9	10 (150)	41.4	61.7
3 (012)	57.5	73.3	11 (180)	85.9	72.6
4 (018)	53.6	71.5	12 (210)	45.1	64.7
5 (024)	43.9	68.7	13 (240)	29.7	38.5
6 (030)	56.9	66.6	14 (270)	1.4	1.9
7 (060)	31.1	42.0	15 (300)	33.0	34.1
8 (090)	4.0	5.2	16 (330)	52.9	62.2

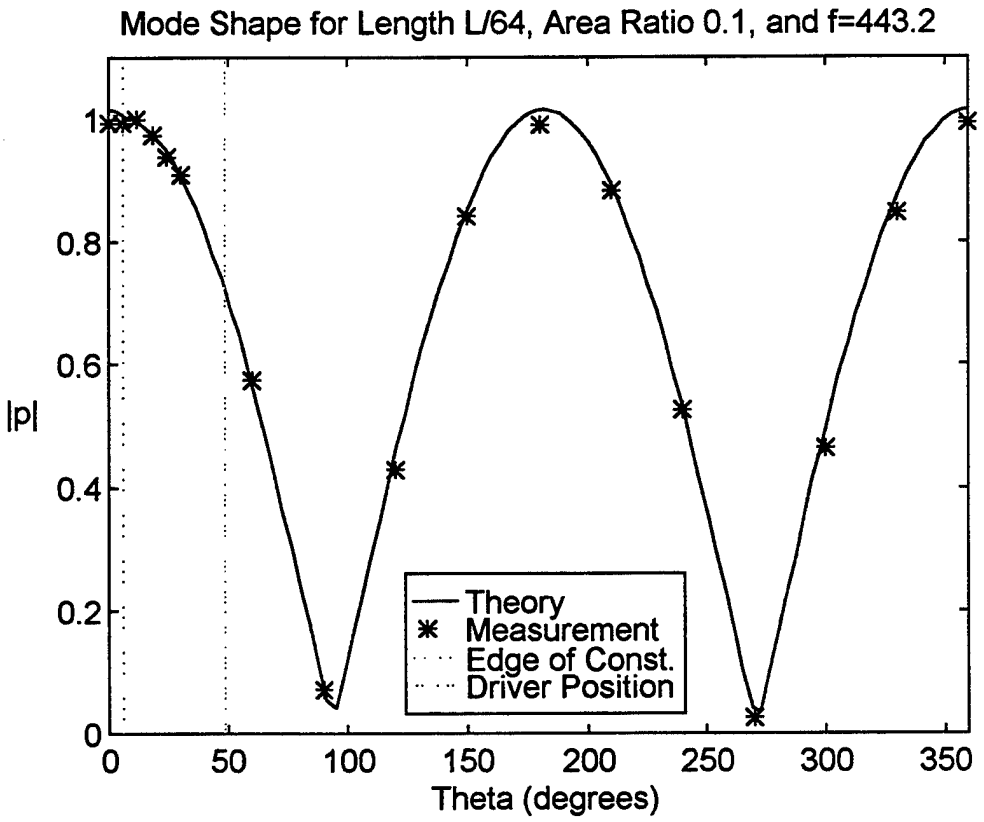

Experiment 10.

Constriction	length: L/ 64 , area ratio: 0.1 , angle from driver:90°				
Resonance frq.: 350.2 Hz		Q: 41	Mode: low		Temp: 24.0°C
Microphone # (θ)	Vrms (mV)	Corrected Data	Microphone # (θ)	Vrms (mV)	Corrected Data
1 (000)	7.1	7.1	9 (120)	17.9	22.4
2 (006)	8.5	8.7	10 (150)	9.2	13.6
3 (012)	13.8	17.4	11 (180)	2.0	1.7
4 (018)	15.8	20.7	12 (210)	7.3	10.4
5 (024)	14.6	22.8	13 (240)	16.0	20.8
6 (030)	21.2	24.8	14 (270)	19.8	26.4
7 (060)	21.9	29.5	15 (300)	28.0	29.3
8 (090)	21.8	28.2	16 (330)	22.3	26.2

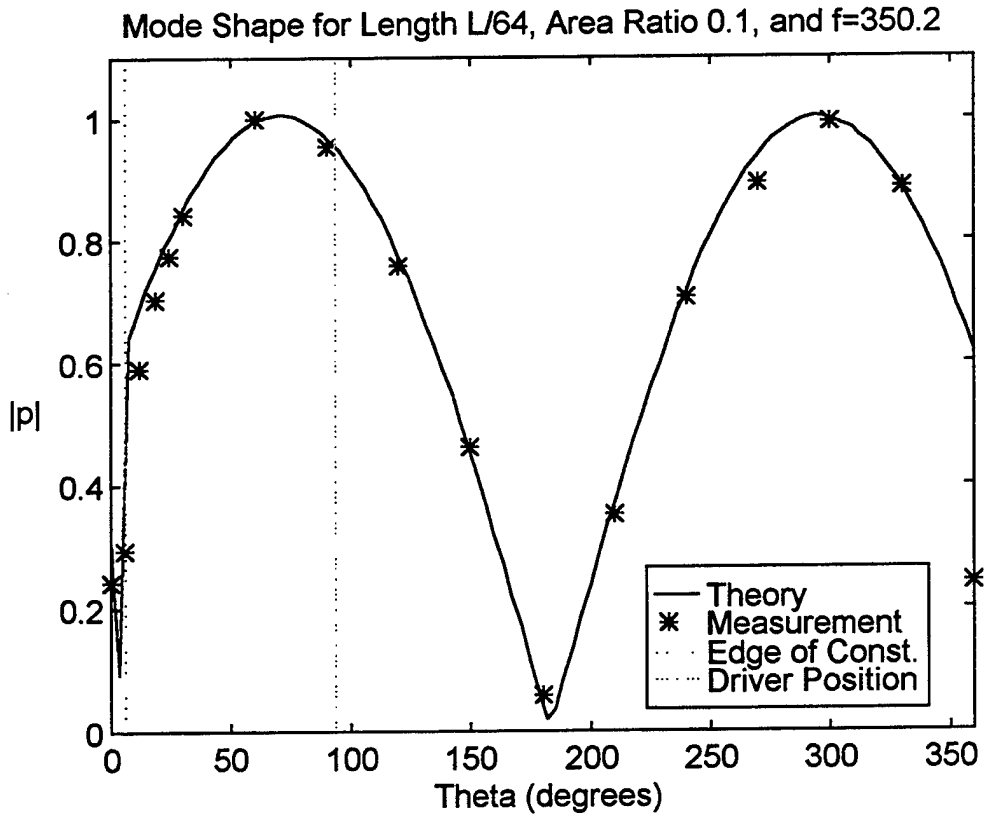

Experiment 11.

Constriction	length: L/ 64 , area ratio: 0.1 , angle from driver:45°				
Resonance frq.: 443.1 Hz		Q: 87	Mode: high		Temp: 24.0°C
Microphone # (θ)	Vrms (mV)	Corrected Data	Microphone # (θ)	Vrms (mV)	Corrected Data
1 (000)	39.8	39.8	9 (120)	13.9	17.5
2 (006)	37.0	38.2	10 (150)	22.7	33.8
3 (012)	31.1	39.7	11 (180)	47.0	39.7
4 (018)	29.1	38.8	12 (210)	24.7	35.4
5 (024)	23.9	37.4	13 (240)	16.1	20.9
6 (030)	31.0	36.3.	14 (270)	0.8	1.1
7 (060)	16.8	22.7	15 (300)	18.6	19.2
8 (090)	2.2	2.9	16 (330)	29.2	34.3

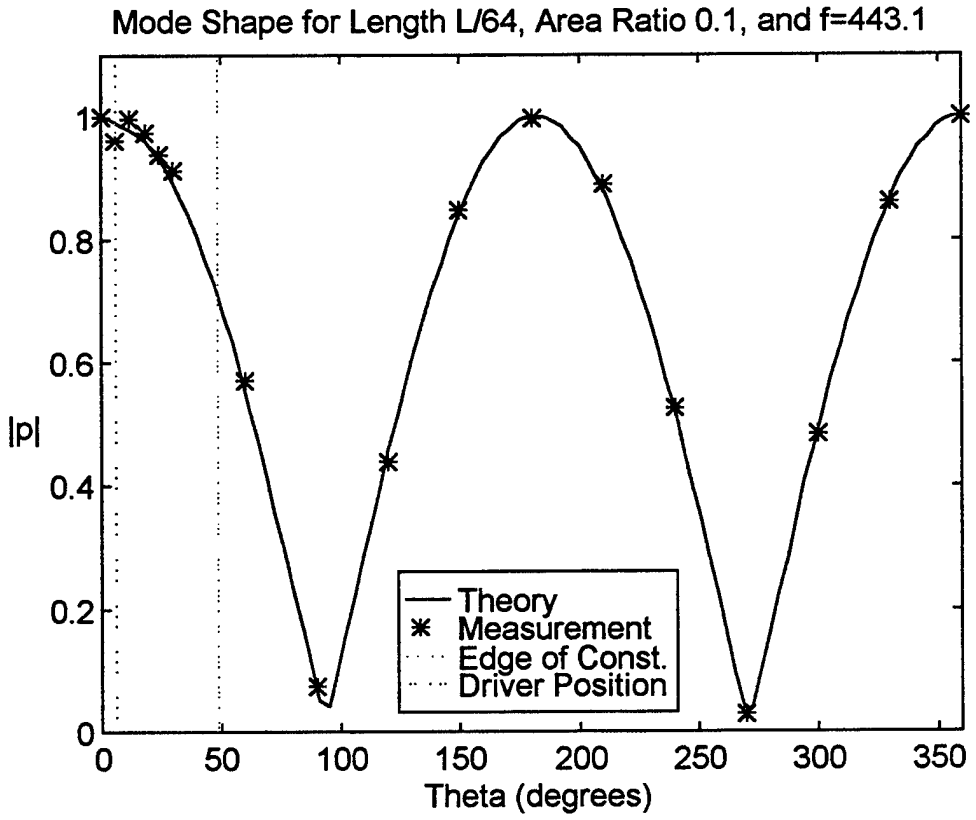

Experiment 12.

Constriction	length: L/ 64 , area ratio: 0.1 , angle from driver:45°				
Resonance frq.: 348.6 Hz		Q: 57	Mode: low		Temp: 24.0°C
Microphone # (θ)	Vrms (mV)	Corrected Data	Microphone # (θ)	Vrms (mV)	Corrected Data
1 (000)	10.0	10.0	9 (120)	25.2	31.6
2 (006)	12.7	13.0	10 (150)	12.8	19.0
3 (012)	20.5	25.9	11 (180)	2.1	1.8
4 (018)	23.3	30.5	12 (210)	11.1	15.8
5 (024)	21.4	33.5	13 (240)	23.4	30.4
6 (030)	31.0	36.3	14 (270)	28.6	38.2
7 (060)	31.6	42.5	15 (300)	39.9	41.8
8 (090)	31.2	40.4	16 (330)	31.5	37.0

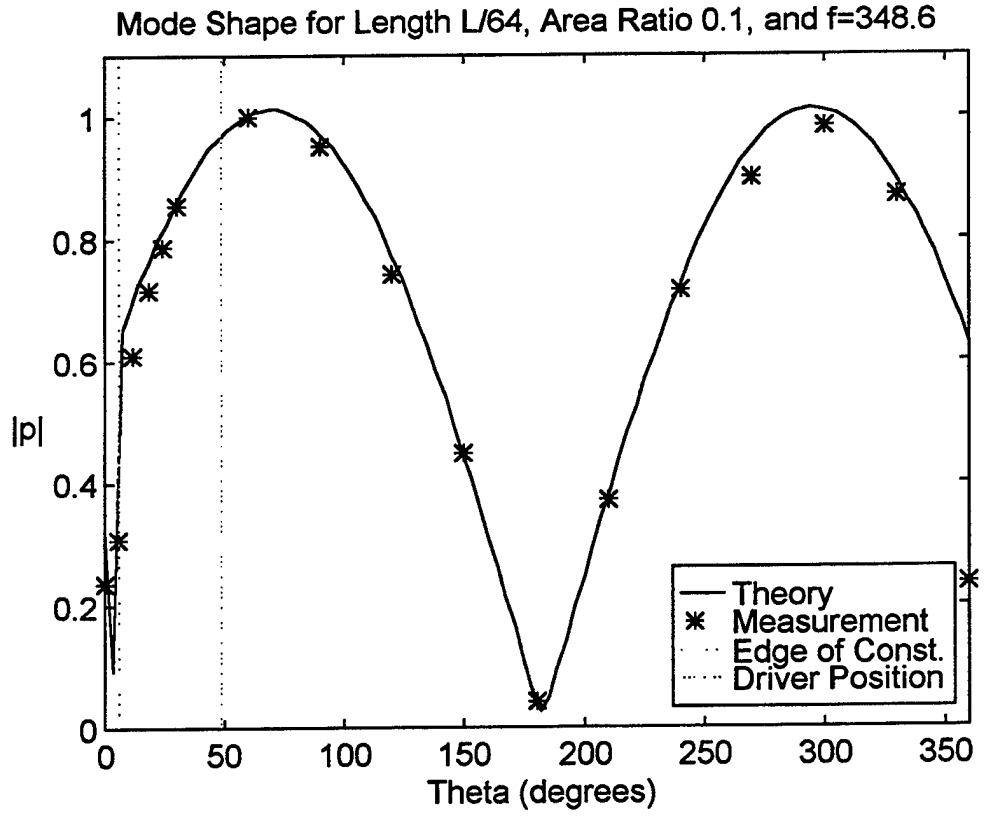

Experiment 13.

Constriction	length: L/ 16 , area ratio: 0.7 , angle from driver:180°				
Resonance frq.: 444.2 Hz		Q: 115	Mode: high		Temp: 21.9°C
Microphone # (θ)	Vrms (mV)	Corrected Data	Microphone # (θ)	Vrms (mV)	Corrected Data
1 (000)	69.3	69.3	9 (120)	15.4	19.4
2 (006)	67.6	69.9	10 (150)	34.7	51.7
3 (012)	55.9	71.3	11 (180)	80.0	67.6
4 (018)	53.1	70.8	12 (210)	46.6	66.9
5 (024)	44.5	69.6	13 (240)	35.4	45.9
6 (030)	58.7	68.7	14 (270)	9.2	12.2
7 (060)	36.8	49.8	15 (300)	22.6	23.3
8 (090)	13.0	17.0	16 (330)	45.6	53.6

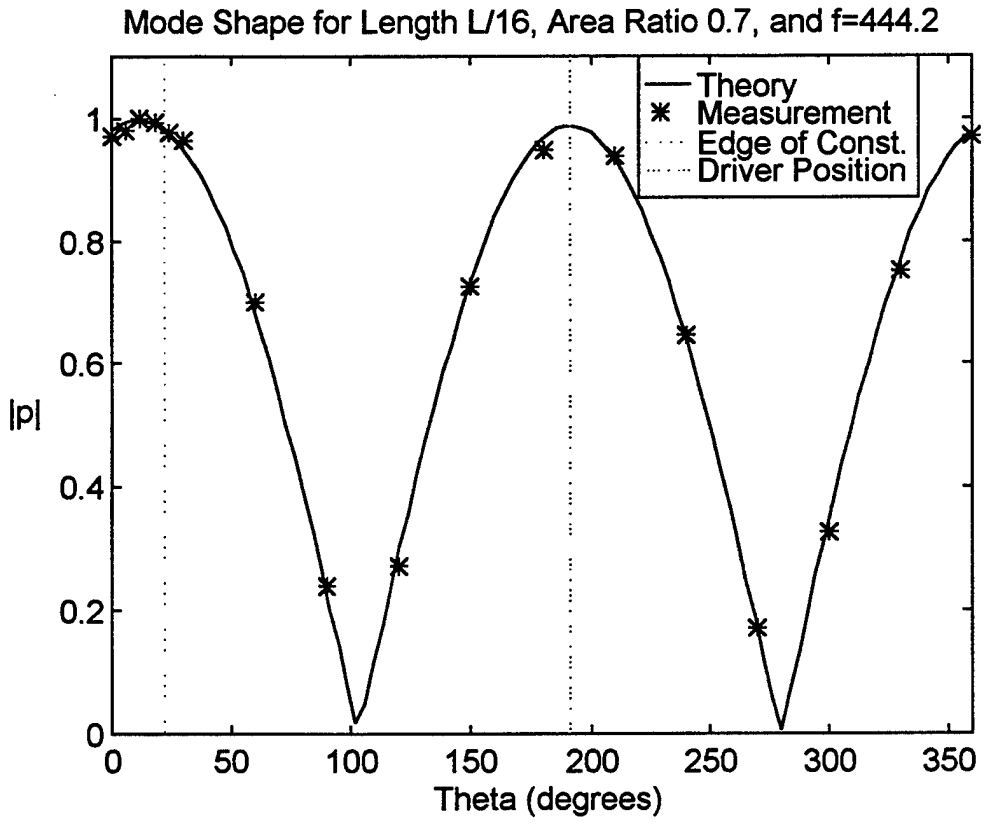

Experiment 14.

Constriction	length: L/ 16 , area ratio: 0.7 , angle from driver:90°				
Resonance frq.: 421.2 Hz		Q: 113	Mode: low		Temp: 22.1°C
Microphone # (θ)	Vrms (mV)	Corrected Data	Microphone # (θ)	Vrms (mV)	Corrected Data
1 (000)	18.3	18.3	9 (120)	54.3	68.2
2 (006)	8.2	8.5	10 (150)	32.5	48.4
3 (012)	1.7	2.2	11 (180)	16.2	13.7
4 (018)	9.2	12.2	12 (210)	16.6	23.7
5 (024)	14.0	21.9	13 (240)	42.7	55.5
6 (030)	26.2	30.7	14 (270)	52.6	69.7
7 (060)	45.0	60.7	15 (300)	68.2	70.6
8 (090)	56.8	74.0	16 (330)	45.0	52.8

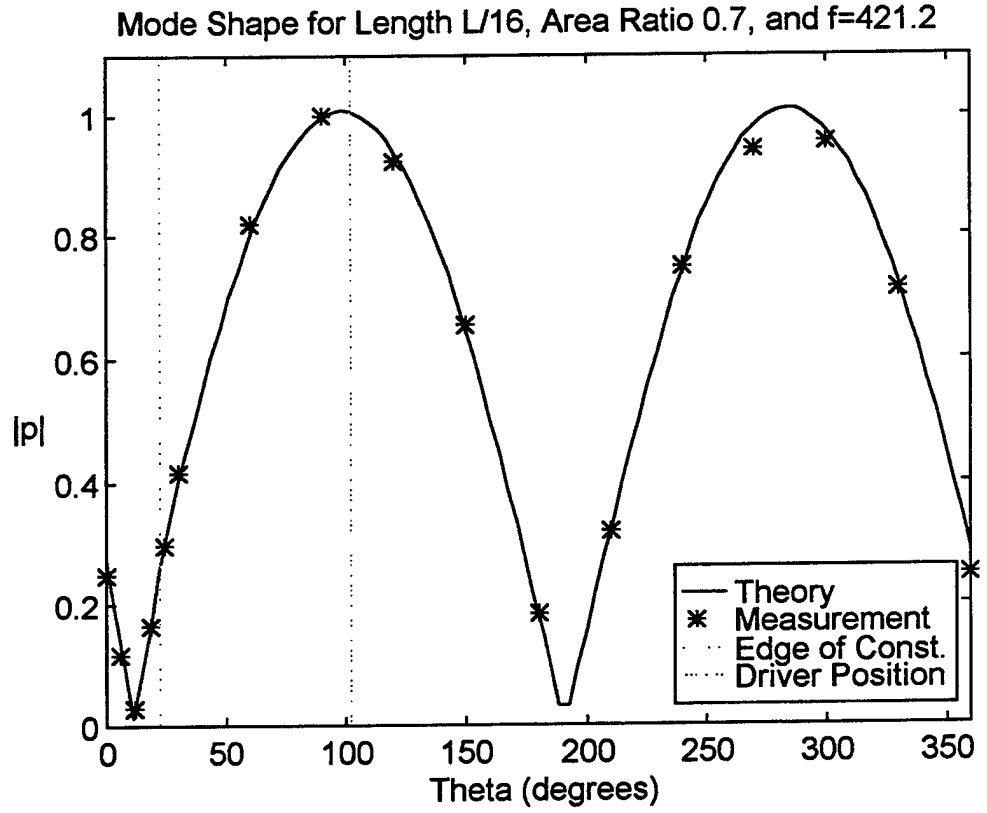

Experiment 15.

Constriction	length: L/ 16 , area ratio: 0.7 , angle from driver:45°				
Resonance frq.: 444.0 Hz		Q: 93	Mode: high		Temp: 22.4°C
Microphone # (θ)	Vrms (mV)	Corrected Data	Microphone # (θ)	Vrms (mV)	Corrected Data
1 (000)	41.6	41.6	9 (120)	10.7	13.5
2 (006)	40.5	41.9	10 (150)	21.5	32.0
3 (012)	33.1	42.2	11 (180)	48.3	40.8
4 (018)	31.5	42.0	12 (210)	27.6	39.6
5 (024)	26.3	41.2	13 (240)	20.6	26.7
6 (030)	34.5	40.4	14 (270)	5.4	7.2
7 (060)	21.4	29.0	15 (300)	15.1	15.6
8 (090)	7.5	9.8	16 (330)	28.2	33.1

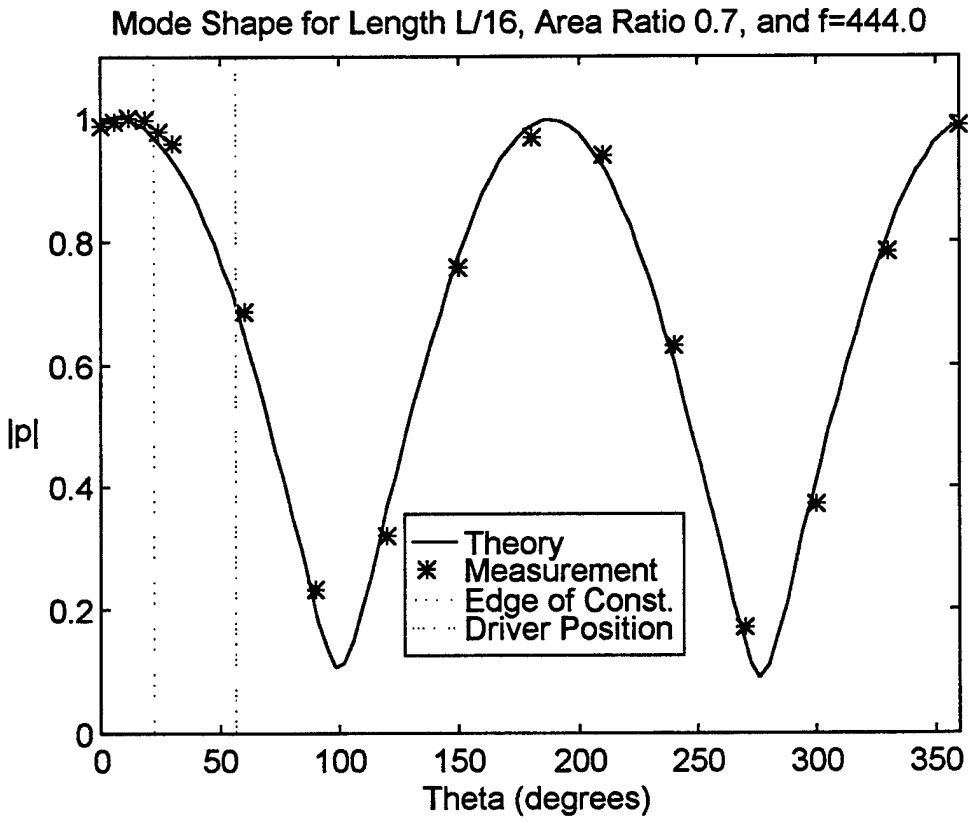

Experiment 16.

Constriction	length: L/ 16 , area ratio: 0.7 , angle from driver:45°				
Resonance frq.: 421.9 Hz		Q: 117	Mode: low		Temp: 22.4°C
Microphone # (θ)	Vrms (mV)	Corrected Data	Microphone # (θ)	Vrms (mV)	Corrected Data
1 (000)	14.3	14.3	9 (120)	43.4	54.5
2 (006)	6.7	6.9	10 (150)	25.8	38.4
3 (012)	3.1	3.9	11 (180)	12.7	10.8
4 (018)	8.4	11.2	12 (210)	14.4	20.6
5 (024)	11.9	18.6	13 (240)	34.9	45.3
6 (030)	21.9	25.6	14 (270)	42.4	56.2
7 (060)	36.7	49.5	15 (300)	54.6	56.5
8 (090)	45.9	59.8	16 (330)	35.7	41.9

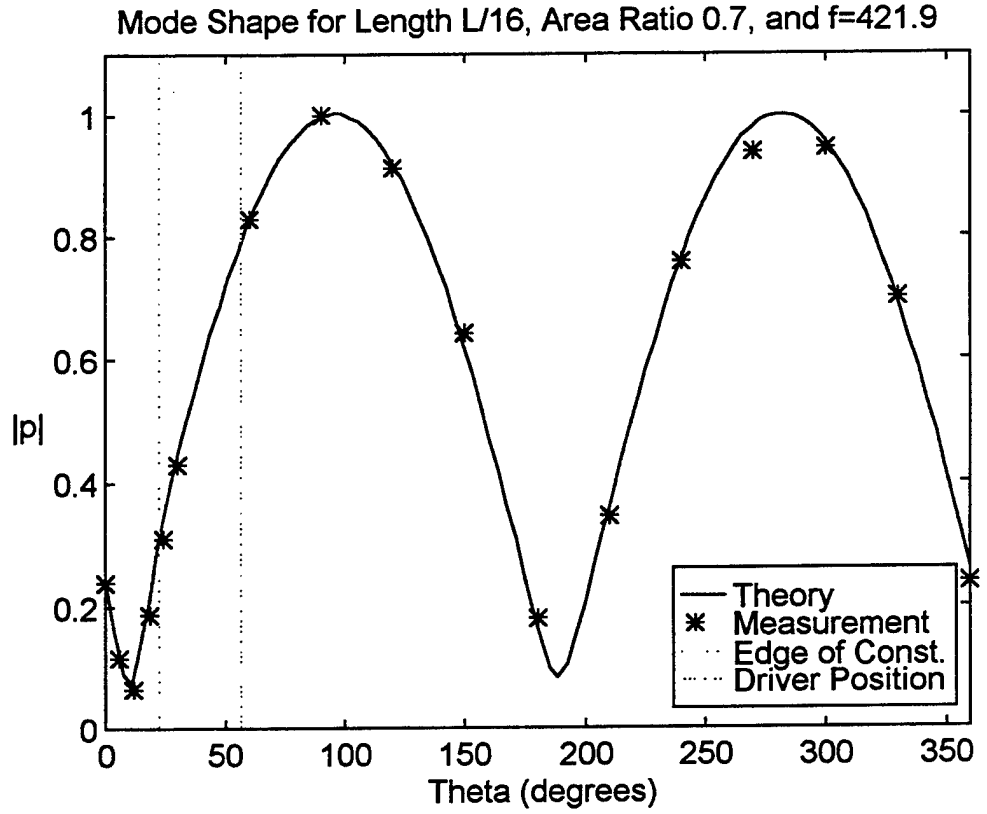

Experiment 17.

Constriction	length: L/ 32 , area ratio: 0.7 , angle from driver:180°				
Resonance frq.: 441.1 Hz		Q: 114	Mode: high		Temp: 23.8°C
Microphone # (θ)	Vrms (mV)	Corrected Data	Microphone # (θ)	Vrms (mV)	Corrected Data
1 (000)	69.4	69.4	9 (120)	20.4	25.7
2 (006)	67.4	69.6	10 (150)	37.5	55.9
3 (012)	55.5	70.8	11 (180)	81.4	68.8
4 (018)	51.5	68.7	12 (210)	45.5	65.2
5 (024)	43.6	68.2	13 (240)	32.4	42.0
6 (030)	56.8	66.5	14 (270)	5.7	7.6
7 (060)	32.8	44.3	15 (300)	26.7	27.6
8 (090)	7.8	10.2	16 (330)	48.0	56.4

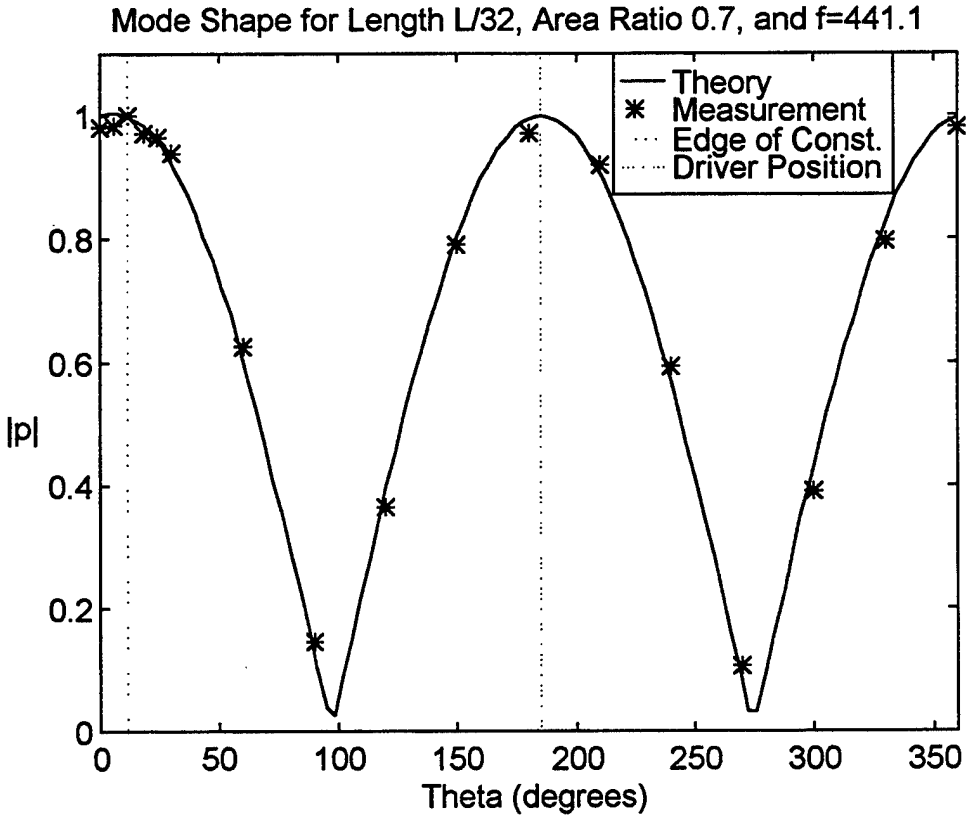

Experiment 18.

Constriction	length: L/ 32 , area ratio: 0.7 , angle from driver:90°				
Resonance frq.: 426.2 Hz		Q: 129	Mode: low		Temp: 21.1°C
Microphone # (θ)	Vrms (mV)	Corrected Data	Microphone # (θ)	Vrms (mV)	Corrected Data
1 (000)	8.7	8.7	9 (120)	57.8	72.6
2 (006)	2.8	2.9	10 (150)	31.7	47.2
3 (012)	10.7	13.6	11 (180)	7.2	6.1
4 (018)	17.2	22.9	12 (210)	24.6	35.2
5 (024)	20.3	31.8	13 (240)	52.1	67.6
6 (030)	34.3	40.1	14 (270)	59.4	78.8
7 (060)	52.8	71.3	15 (300)	71.9	74.4
8 (090)	63.5	82.8	16 (330)	42.4	49.8

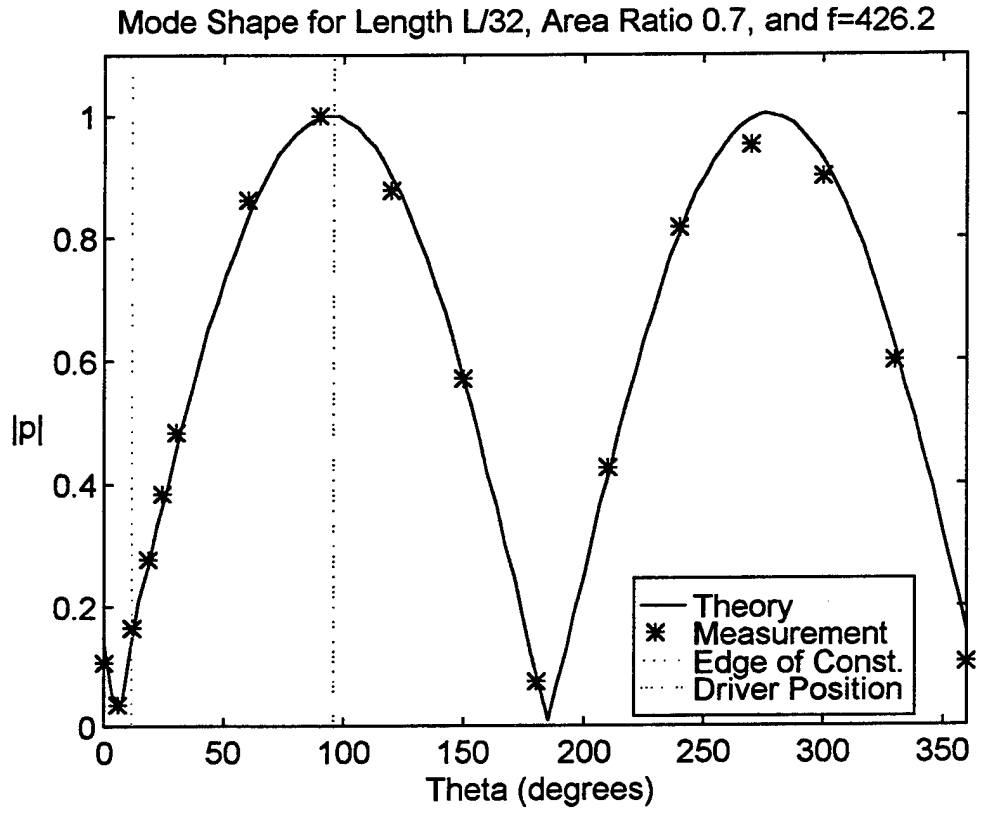

Experiment 19.

Constriction	length: L/ 32 , area ratio: 0.7 , angle from driver:45°				
Resonance frq.: 439.3 Hz		Q: 101	Mode: high		Temp: 21.6°C
Microphone # (θ)	Vrms (mV)	Corrected Data	Microphone # (θ)	Vrms (mV)	Corrected Data
1 (000)	43.4	43.4	9 (120)	14.6	18.4
2 (006)	42.0	43.4	10 (150)	24.0	35.8
3 (012)	34.3	43.8	11 (180)	51.6	43.6
4 (018)	31.7	42.3	12 (210)	27.9	40.0
5 (024)	26.7	41.8	13 (240)	19.8	25.7
6 (030)	34.8	40.7	14 (270)	5.8	7.7
7 (060)	20.2	27.3	15 (300)	18.8	19.4
8 (090)	7.0	9.1	16 (330)	30.6	36.0

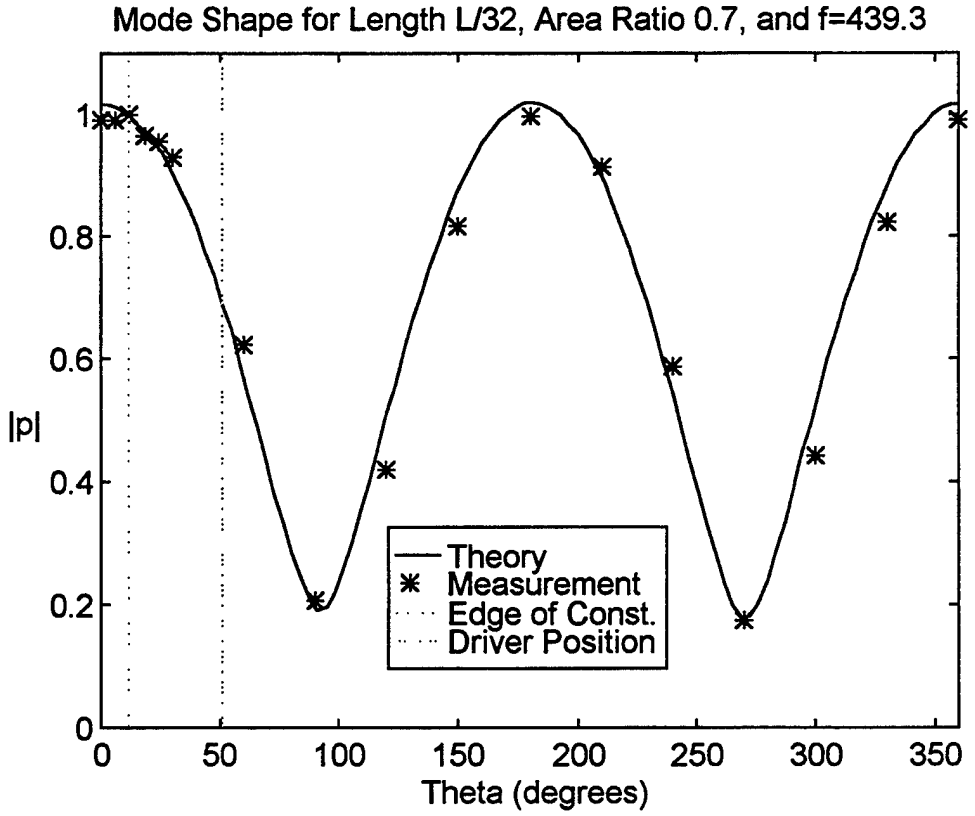

Experiment 20.

Constriction	length: L/ 32 , area ratio: 0.7 , angle from driver:45°				
Resonance frq.: 426.9 Hz		Q: 125	Mode: low		Temp: 21.6°C
Microphone # (θ)	Vrms (mV)	Corrected Data	Microphone # (θ)	Vrms (mV)	Corrected Data
1 (000)	8.7	8.7	9 (120)	42.3	53.1
2 (006)	6.5	6.7	10 (150)	23.2	34.5
3 (012)	9.5	12.1	11 (180)	9.6	8.1
4 (018)	13.7	18.2	12 (210)	19.1	27.4
5 (024)	15.7	24.5	13 (240)	38.7	50.2
6 (030)	26.1	30.5	14 (270)	43.6	57.8
7 (060)	39.2	52.9	15 (300)	52.5	54.3
8 (090)	46.7	60.9	16 (330)	30.9	36.3

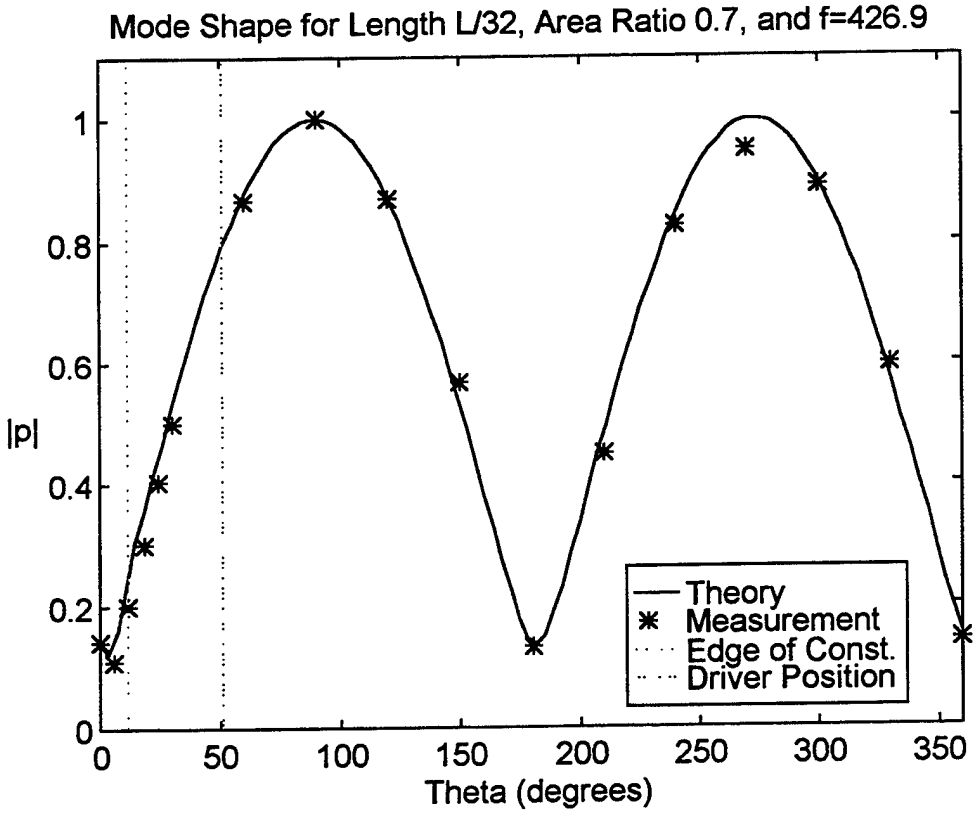

LIST OF REFERENCES

1. L. E. Kinsler, A. R. Frey, A. B. Coppens and J. V. Sanders, "Fundamentals of Acoustics," Third Edition, John Wiley & Sons, Inc., 1982.

2. Hewlett Packard, "HP 3562A Dynamic Signal Analyzer Operating Manual," Hewlett Packard.

3. A. D. Pierce, "Acoustics-An Introduction to its Physical Principles and Applications," J. Acoutical Society of America, 1989.

4. G. W. Swift, "Thermoacoustic Engines," J. Acoutical Society of America 84, 1988.

5. A. A. Atchley and R. T. Muehleisin, "Development of an Active Impedance Load," Proceedings of Noise-Con, 1997.

6. P. M. Morse and K. U. Ingard, "Theoretical Acoustics," Princeton University Press, Princeton NJ, 1968.

7. R. T. Muehleisin and D. C. Swanson, "The Use of Modal Coupling Matrices in Solving Size Discontinuity Problems," In preparation.

DISTRIBUTION LIST

1. Defense Technical Information Center..... 2
   8725 John J. Kingman Road., Ste 0944
   Ft. Belvoir, VA 22060-6218

2. Dudley Knox Library.....2
   Naval Postgraduate School
   411 Dyer Rd.
   Monterey, CA 93943-5101

3. Professor Anthony Atchley, Code PH/Ay.....2
   Department of Physics
   Naval Postgraduate School
   Monterey, CA 93943-5101

4. Major Lin, Hsiao-Tseng.....2
   Vehicle Engineering Department, Chung-Cheng Inst. Of Tech.
   Ta-Shi, Tao-Yuan, 33509
   Taiwan, R.O.C.

5. Dr. Ralph T. Muehleisin.....1
   Department of Physics
   Naval Postgraduate School
   Monterey, CA 93943-5101

6. LCDR Choe, Seok Yun.....2
   Seoul, Korea
   Seoul City, Yeong-Deoung-Po Gu,
   Yoi-Do Dong, Sam-Ik APT D-1201